2.3.5. **Wave Field in Crystal**

Formation of the wave field has two cases in the crystal, as it already (2.2.6) described. One is mutual interference of two diffracted waves and mutual interference of two transmitted waves connected with tie points 1 and 2 (pendellösung beat). Second is interference with the diffracted wave and the transmitted wave connected with the same tie point (standing wave). Conventionally, the standing wave in the crystal has been discussed in the category of SIA. However, this study will be examine over entire region from $q= 0$ to 1.

(i) Phase of the pendellösung beat in $q= 0$ and $q= 1$

When the difference is in the wave number of the wave from two tie points, the beat is generated and the pendellösung beat is observed. As shown in Fig.2.8(a),(b) and Fig.2.9(a), (b) in $q= 0$, the phase of the pendellösung beat is reverse at the diffracted intensity and the transmitted intensity. On the other hand, as shown in Fig.2.8(e), (f) and Fig.2.9(e), (f) in $q= 1$, the phase of the pendellösung beat is the same at the diffracted intensity and the transmitted intensity. Thus, in $q= 0$ and $q= 1$, the phase of the pendellösung beat has the big difference. Although it can understand the phenomenon that becomes an antiphase for $q= 0$, from the energy conservation, it cannot understand intuitively the phenomenon that becomes an in-phase for $q= 1$. We consider the origin of this difference from equations. In $q= 0$ and $q= 1$,

the following relationship is obtained from (2.95) and (2.97) between the diffracted intensity and the transmitted intensity. In (2.95) for q= 0, the diffracted intensity is the remainder which subtracted the transmitted intensity from the remained intensity(exp) by mean-absorption. And, in (2.97) for q=1, the diffracted intensity is the remainder which subtracted the mean-absorption from the transmitted intensity. Therefore, the phase of the pendellösung beat of the diffracted intensity become opposite to the transmitted intensity for q= 0, and is the same for q= 1.

(ii) A pendellösung beat and crystal structure factor

Assuming the period of the pendellösung beat to be l, l and s have the relationship in following equation

$$s=\frac{\pi}{l|\sqrt{Q}|}. \qquad (2.124)$$

l can be determined the high accuracy by experiment. The reason is because the period (measured as distance) of the equal thickness interference fringes, and the period (by measured as angle) of the pendellösung beat seen on the rocking curve can measure with high precision. Since l is determined precisely experimentally, s is also determined from (2.124) precisely. Conventionally, the precision determination of the crystal structure factor has been performed from measurement of the s with the application of SIA. Following, the justification of the method is examined.

The following equation is established between s of this study and s' of SIA

$$\frac{s}{s'}=\frac{1}{\sqrt{1-q}}. \tag{2.125}$$

If $|\chi_{hr}|>>|\chi_{hi}|$, $q \approx 0$ will result. Therefore, s of this study corresponds with s' of SIA. If s in (2.124) is s' in SIA, $|\chi_{hr}|$ will be obtained from the measurement value of s'. $|F_{hr}|$ is calculated from $|\chi_{hr}|$. That is, if SIA, the real part of the crystal structure factor is obtained from observation of the period of a pendellösung beat, and the imaginary part $|F_{hi}|$ will not be obtained. Since the pendellösung beat can also observe the diffraction of only $|F_{hi}|$ in this theory, the conclusion of this theory and the conclusion of SIA is not in agreement. The amplitude of the crystal structure factor is obtained from s in this theory, and it cannot choose and request which of $|F_{hr}|$ or $|F_{hi}|$. The error of $|F_{hr}|$ by SIA is examined from this theory, . The range of $|F_{hi}|/|F_{hr}|$ by SIA is 0.1 or less. This is $q<$ 0.01 and $s/s'<1.005$. Therefore, when $|F_{hi}|/|F_{hr}|=0.1$, determining $|F_{hr}|$ from s' obtained by (2.124) will include 0.5% of the error. The result not mean the precision determination of $|F_{hr}|$. If $|F_{hi}|/|F_{hr}|=1$, $q=0.5$ and $s/s'=1.414$ from (2.125). That is, $|F_{hr}|$ which is obtained by SIA includes about 40% of the error.

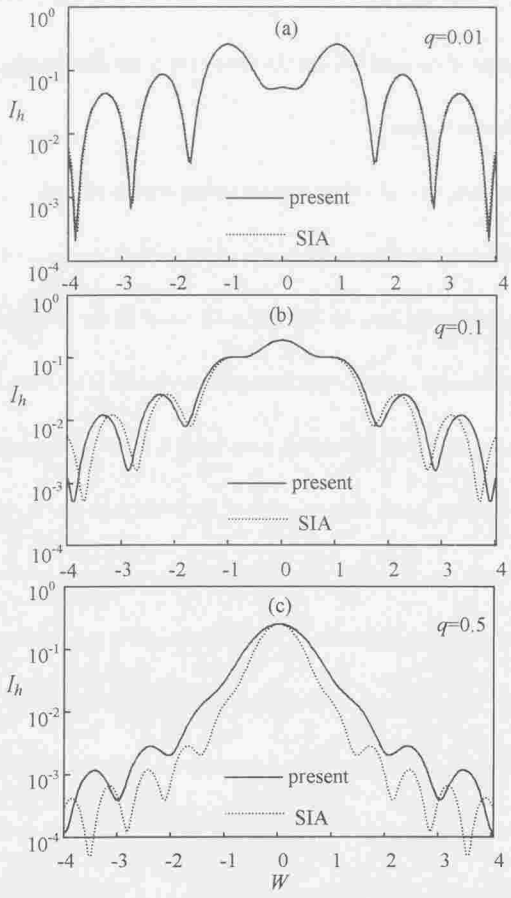

Fig 2.21 The rocking curves of the diffracted wave in the symmetric Laue case for $sH=\pi$. (a) $q = 0.01$; (b) $q = 0.1$ and (c) $q = 0.5$.

The rocking curve obtained by the SIA and the present theory are shown in Fig. 2.21.

Here, $sH = \pi$, and (a) q=0.01, (b) q=0.1 and (c) q=0.5. Solid lines shows the result obtained

by (2.90), and, dotted lines shows the result obtained using W' of (2.50) in SIA. In (a), the difference of the period of the solid line and the dotted line is not seen clearly. However, in (b) and (c), the difference is clear.

(iii) Pendellösung beat and anomalous transmission (disappearance of beat)

At $W= 0$, the diffracted intensity which changes q and sH and was obtained is shown in Fig.2.22. In the pendellösung beat of the diffracted wave, if the amplitude of waves connected with two tie points differs or the absorption coefficient to two waves differs, the amplitude of the node of beats will not become zero. In $q= 0$, two imaginary solutions of the dispersion surface becomes equal, and the value of the solution is zero in $\chi_{0i}=0$, and is negative fixed value in $\chi_{0i} \neq 0$. For this reason, since two waves receive the same absorption (the zero absorption are included), the amplitude of the node of the pendellösung beat in the diffracted wave is zero (the thin dotted line and thick dashed line in Fig.2.22). However, in $0<q<1$, two imaginary solutions of the dispersion surface differs, and absorption of two waves differs. For this reason, the amplitude of the node in the beat does not become zero (the thick dot dashed line and thick solid line in Fig.2.22). These phenomena are seen also like the pendellösung beat on rocking curves of (a),(b) and (c) in Fig.2.8.

In Fig.2.22, when sH becomes large, if q approaches 1, the pendellösung beat in $W= 0$ disappears and, moreover, I_h becomes to converge on 0.25. With increase of sH, since one wave of the tie point is absorbed greatly and the intensity becomes weak, this pendellösung

beat disappears (anomalous absorption). Although another diffracted wave becomes to converges on 0.25, this diffracted wave is not absorbed (anomalous transmission). In q= 1,

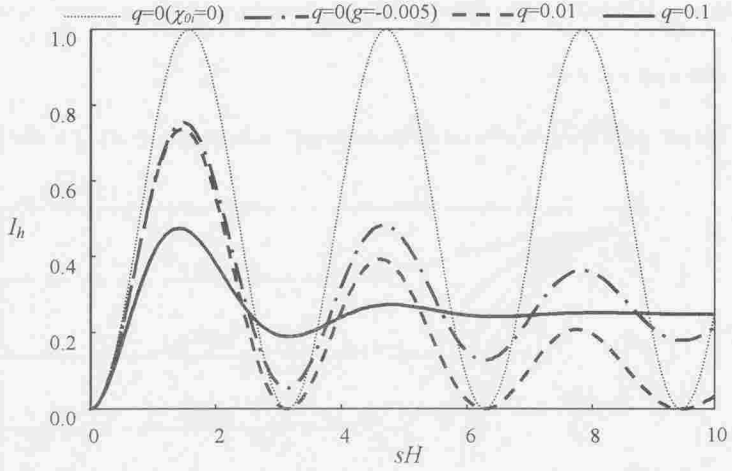

Fig 2.22 The Pendellösung beats of the diffracted wave in the symmetric Laue case for q= 0, 0.01 and 0.1 when δ = 0, W = 0.

even when sH changes at W= 0, the pendellösung beat is not seen. The following is examined the reason.

In q= 1, real part of solution Y in the dispersion surface is zero in $|W|<1$. Therefore, there is no difference in the wave number of the wave by two tie points. For this reason, the pendellösung beat disappears in $|W|<1$. The rocking curve of the transmitted intensity which changed sH is shown in Fig.2.23. If sH increases, although the period of the pendellösung beat in $W>1$ will become small, the pendellösung beat does not appear in $W<1$. That is, since the real part of the solution of the dispersion surface is zero in q= 1, the pendellösung

beat cannot observe in $W< 1$. Two conclusions will be obtained from the above consideration. In $0<q<1$, if sH increases, the pendellösung beat will disappear by the anomalous absorption. And in $q= 1$, since there is no difference in the wave number of two waves, there is also no pendellösung beat in $W< 1$.

The process of disappearance for the pendellösung beat at $W= 0$ to $q= 0$ to 1 is shown in

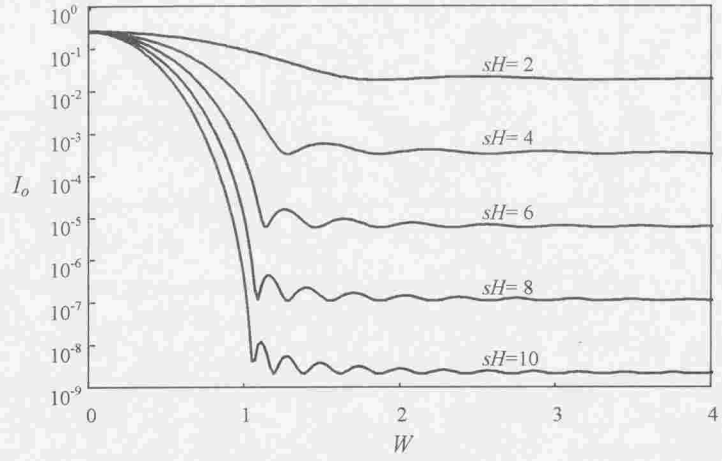

Fig 2.23 The rocking curves of the transmitted wave in the symmetric Laue case for $q= 1$ and different values of sH.

Fig.2.24. Within a crystal, (a) shows that the amplitude of the pendellösung beat does not decrease, when there is no absorption ($q= 0$). However, if there is absorption in $q= 0$, (b) at inside of the crystal shows that the amplitude of the pendellösung beat becomes small and the amplitude of the node on the beat is zero. (c) is in case of $q= 0.1$. Only the first pendellösung beat is visible and the amplitude of the node on the beat does not become zero.

But, the amplitude of the wave does not decrease at inside of the crystal, and it becomes fixed value, and the anomalous transmission is shown. (d) is in case of q= 1.

There is no pendellösung beat near the crystal surface. The transmitted wave decreases

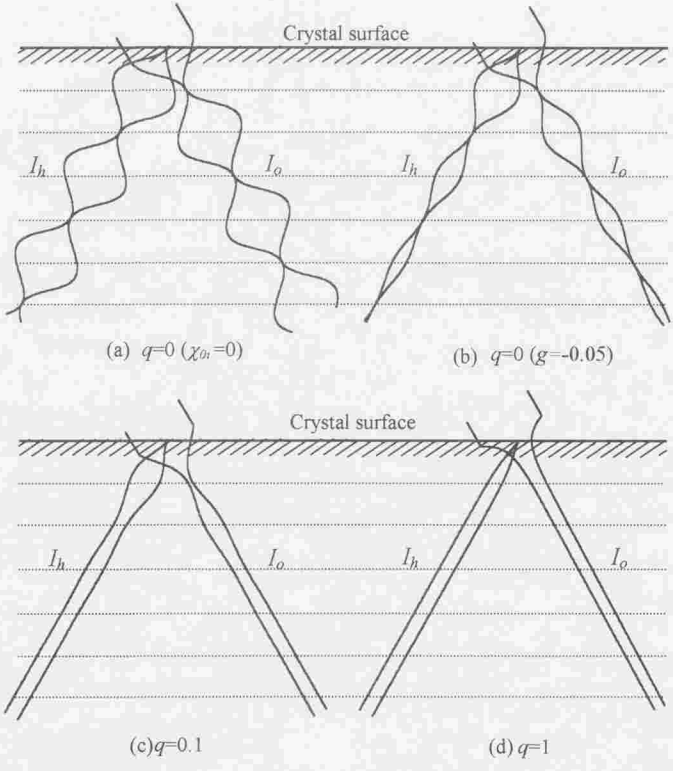

Fig 2.24 The Pendellösung beats in the crystal when W=0.

remarkably near the crystal surface, and the diffracted wave increases. When sH increases from 3or more in Fig.2.7, the intensity converged on fixed value like (c), and the diffracted

wave and the transmitted wave show the anomalous transmission.

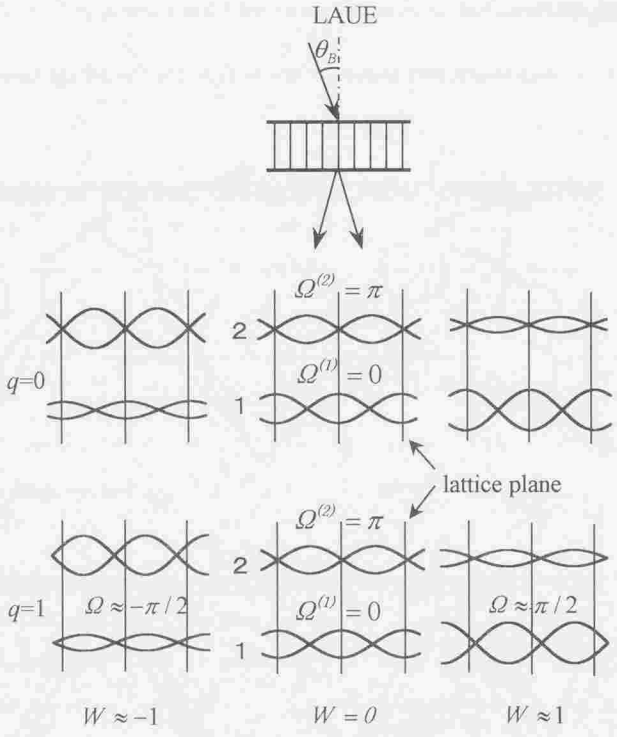

Fig 2.25 The standing waves in the symmetric Laue case.
The upper figures for q=0 and the lower for q=1.

(iv) Standing wave

In this section, the standing wave in the crystal is examined in q= 0 to 1. Batterman and Cole(BC) carried out the study of what wave field is shaped on the lattice surface in the

crystal by SIA. The wave field shown by (2.92) is given by interference with the diffracted wave and the transmitted wave from one tie point. Approximation as SIA is not given (2.92).

a) *In case of* q= 0

Electric displacements ($D_o^{(j)}, D_h^{(j)}$) in the tie point at W= 0 are calculated. If $\alpha_{hr} = \pi$ and $g_0 = -\infty$, $D_o^{(1)} = D_o^{(2)} = E_0 / 2$ are obtained from (2.73). And $D_h^{(1)} = -D_h^{(2)} = E_0 / 2$ are obtained from (2.60). Therefore, $\Omega^{(1)} = 0$ from $R^{(1)} = 1$ in the tie point 1. In the tie point 2, $\Omega^{(2)} = \pi$ from $R^{(2)} = -1$. This result is shown in the upper row of Table 2.2.

In W= 0, the field intensity $I^{(j)}(x)$ in the crystal is composition with $\boldsymbol{D}_0^{(j)}(\boldsymbol{r})$ and $\boldsymbol{D}_h^{(j)}(\boldsymbol{r})$, and obtains the following equation from (2.92)

$$I^{(j)}(x) = |D^{(j)}(x)|^2_{(W=0)} = \frac{|E_o|^2}{2} \exp(-\frac{\mu z}{\cos\theta_B})[1 + (-1)^{j-1} \cos(\frac{2\pi x}{d})]. \qquad (2.126)$$

Where, distance x has the same direction as reciprocal-lattice vector $\boldsymbol{h}$. The inside of [ ] expresses the standing wave which makes lattice plane interval d. In $\alpha_{hr} = \pi$, the magnitude of the [ ] is maximum 2 for j= 1 in the lattice plane, and is the minimum value 0 for j= 2. Behavior of this standing wave is shown in Fig. 2.25. That is, the standing wave of the tie point 1 in Bragg conditions(W=0) has the antinode in the lattice plane, and the standing wave of the tie point 2 has a node there. Conversely, on condition that α_{hr} = 0, the standing wave of the tie point 1 has the node in the lattice plane, and the standing wave of the tie point 2 has the antinode there. That is, the relationship between the node and the antinode is

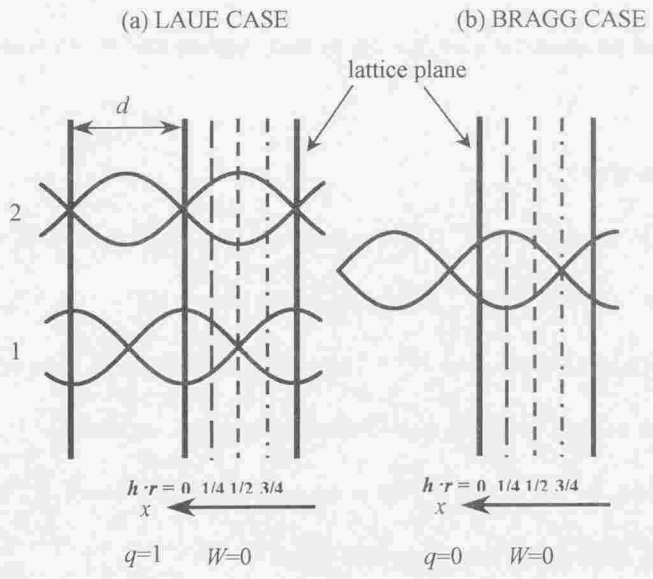

Fig.2.26 The plane(x=0, d/4, d/2 ,3d/4) in the unit cell.
(a) Laue case. (b) Bragg case.

reversed for $\alpha_{hr} = \pi$.

$I^{(j)}(x)$ is examined for W dependence. In order to examine behavior of the wave field of (2.92), as shown in Fig. 2.26, four planes of x (=0, d/4, d/2, 3d/4) between lattice planes are considered. Here, χ_{hr} is π and $I^{(j)}(x)$ is dependent on the depth z from the crystal surface. In q= 0 and g=–0.1, $I^{(j)}(x)$ is shown in Fig. 2.27. $I^{(1)}(x)$ of the tie point 1 is (a), (c) and (e), and $I^{(2)}(x)$ of the tie point 2 is (b), (d) and (f). In Fig.2.27(a), $I^{(1)}(0)$ (solid line) in the lattice plane (x= 0) becomes large gradually, when W approaches from negative to 0, and

it is 1.0 at W= 0.

$I^{(1)}(0)$ obtains maximum (1.457) at the positive side of W. And if W increases, $I^{(1)}(0)$ will become average value 1.0. $I^{(1)}(d/2)$ (dotted line) in the center of lattice planes(x=d/2) takes the maximum value (0.043) at W=−1, and takes the minimum value 0 at W= 0. And $I^{(1)}(d/2)$ approaches average value 1.0 at the positive side of W. In x=d/4 (dashed line) and x= 3d/4(dot dashed line), $\cos(2\pi x/d)$ of (2.126) is zero. Therefore, $I^{(1)}(x = d/4 \text{ or } 3d/4)$ at W= 0 is 0.5, and shows the middle change in cases of x= 0 and x=d/2. In Fig.2.27(b), $I^{(2)}(0)$ of the tie point 2 has reversed change of the tie point 1 with W. However, $I^{(2)}$ is change which replaces $I^{(1)}$ for x= 0 and x=d/2. Moreover the phase of $I^{(j)}(x)$ in d/4 and 3d/4 differs π in tie points 1 and 2.

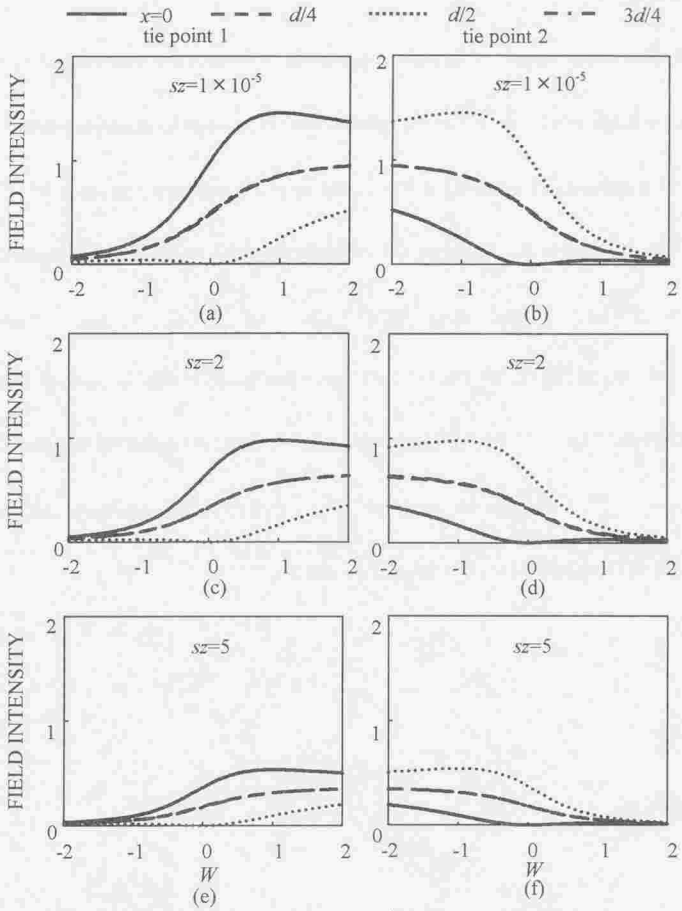

Fig.2.27 The change of the wave field $I^{(j)}(x)$ for x=0, d/4, d/2 and 3d/4 in the symmetric Laue case for q=0, g=-0.1 and $\alpha_{hr}=\pi$.

The effect with absorption appears in the term of exp in (2.92). $I^{(j)}(x)$ which increased sz gradually from the crystal surface is shown in the Fig 2.27 (from (c) to (f)). Behavior of I in tie points 1 and 2 is decreasing simply with the increase in sz like change of the Poynting

vector.

b) *In case of* q= 1

If $\alpha_{hi} = \pi$, q= 1, then $\overline{\chi_h}/\chi_{-h} = i$. $R^{(j)}$ obtains the following relationship from (2.70)

$$R^{(j)} = i\left[W + (-1)^j \sqrt{W^2 - 1} \right]. \qquad (2.127)$$

The phase angle $\Omega^{(j)}$ of this $R^{(j)}$ is $-\pi/2$ ($R^{(1)}$= $R^{(2)}$=$-i$) at W=−1. And at W= 1, the phase angle becomes $\pi/2$ ($R^{(1)}$= $R^{(2)}$=i) . Therefore, these phase angles do not have difference of the tie point. However, at W= 0, (1)$\Omega^{(1)}$=0 ($R^{(1)}$=1), and (2)$\Omega^{(2)}$=π ($R^{(2)}$=−1), these are shown in the under row Table 2.2. In this way, Ω differs by tie points 1 and 2. If $\alpha_{hi} = 0$, $\overline{\chi_h}/\chi_{-h} = -i$. Therefore, at W= −1, $\Omega^{(j)} = \pi/2$, and $\Omega^{(j)} = -\pi/2$ at W= 1,and at W=0, $\Omega^{(1)} = \pi$ and $\Omega^{(2)} = 0$ at W= 0. Thus, the phase angle of the standing wave in $\alpha_{hi} = 0$ is opposite to the phase angle in $\alpha_{hi} = \pi$. In q= 0, the amplitude of the wave field in the crystal decreases simply as the deepness become to deep from the crystal surface, and the phenomenon of the anomalous transmission was not looked at by the change of thickness.

In q= 1, in order to investigate the relationship between the standing wave and the anomalous transmission, the term of exp in (2.126) will be examined. If g_0=–1, when W changes with –1, 0 and 1, the term of exp of (2.92) changes as shown in Table 2.3. The wave field of tie points 1 and 2 receives the mean absorption in $|W|$=1 so that it may be understood from the imaginary part of the dispersion surface. And, the wave field of the tie point 1 receives the strong absorption which is twice the mean absorption at W= 0. However, an absorption coefficient for the tie point 2 at W= 0 is zero and the wave field does not have any absorption. The wave field of the tie point 2 which has the node in the lattice plane has small absorption unusually, and the wave field of the tie point 1 which has the antinode in the lattice plane has large absorption unusually. BC showed this effect from SIA theory. The conclusion of BC is the same also in q= 1.

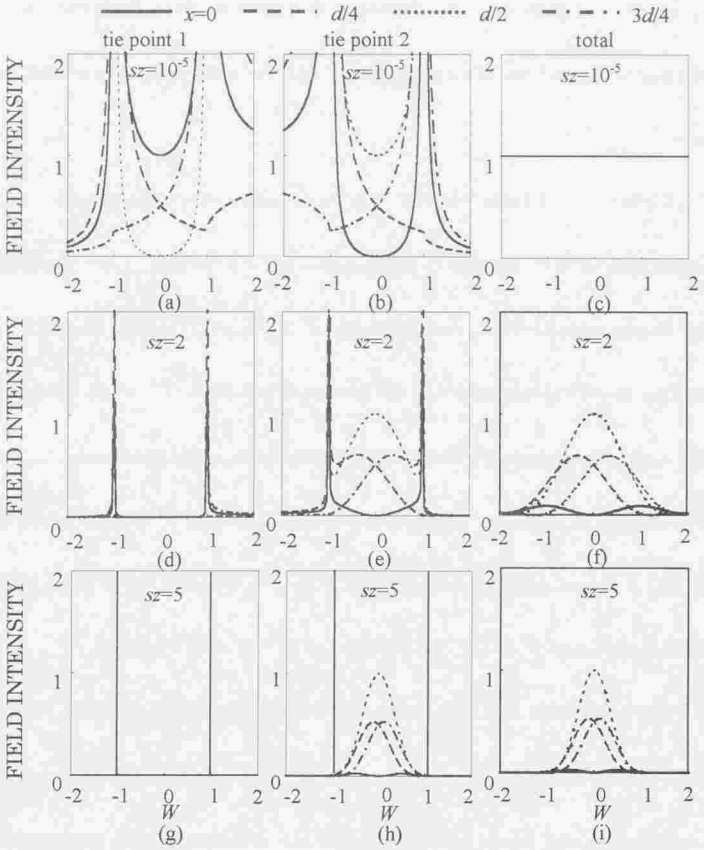

Fig.2.28 The change of the wave field $I^{(j)}(x)$ for x=0, d/4, d/2 and 3d/4 in the symmetric Laue case for q=1, and . TP1:(a)sz=1×10^{-5}, (d)sz=2 and (e)sz=5. TP2: (b)sz=1×10^{-5}, (e)sz=2 and (h)sz=5. Total field: (c)sz=1×10^{-5}, (f)sz=2 and (i)sz=5. Note that there is no divergence in the total field. (TP: Tie point).

In this following paragraph, the field intensity $I^{(j)}(x)$ is explained as sz, x and W dependence. Fig. 2.28 is results for q=1. Figures(a), (b) and (c) are near the crystal surface. $I^{(j)}$ in tie points 1 and 2 diverge at $|W|$=1. However, as composition ($|D^{(1)}(x)+D^{(2)}(x)|^2$) of

$I^{(1)}(x)$ and $I^{(2)}(x)$ is shown in (c), there is no divergence at $|W|=1$. Since they have the opposite phase of wave fields of tie points 1 and 2, the divergence negates each other and it disappears.

In Fig.2.28(a), $I^{(1)}(0)$ (solid line) at $x=0$ in the tie point 1 becomes large gradually as W approaches from -2 to -1, and after diverging at $W=-1$, it will becomes 1 (antinode) at $W=0$ and will diverge again at $W=1$, then approaches 1. Although $I^{(1)}(d/2)$ (dotted line) at $x=d/2$ shows the same change as $x=0$, it will become zero at $W=0$. $I^{(1)}(d/4)$ (dashed line) at $x=d/4$ changes from maximum to the local minimum value, when W changes -1,0,and 1, and if W becomes large further, will approach average value 1.0. $I^{(1)}(10^{-5},3d/4,W)$ (dot dashed line) at $x=3d/4$ changes conversely with W to $I^{(1)}(10^{-5},d/4,W)$ in $|W|<1$. That is, there is the relationship of $I^{(1)}(10^{-5},3d/4,W)=I^{(1)}(10^{-5},d/4,-W)$ in $|W|<1$.

The W dependability of $I^{(2)}(x)$ in the tie point 2 carries out change which $I^{(1)}(x)$ in the tie point 1 reverse with W, as shown in a Fig.2.28(b). However, field intensities in $x=0$ and $x=d/2$ interchanges, and that in $x=d/4$ and $x=3d/4$ also interchanges. And, composition of two wave fields with tie points 1 and 2 is a constant value 1.0 to W, as shown in (c). $I^{(j)}(x)$ at $sz=2$ are shown in (d), (e) and (f), and at $sz=5$ are shown in (g), (h) and (i). As $sz>2$, $I^{(1)}(x)$ in the tie point 1 decreases remarkably, and it is not seen in (g), except $|W|=1$. However, as shown in (e) and (h), $I^{(2)}(x)$ of the tie point 2 at a near $W=0$ does not decrease, even when sz increases . Therefore, the most of field intensities in (f) and (i) is the

component of the tie point 2.

The above dependability of x and sz is understood from change of the standing wave in the crystal surface and the term of the absorption for every tie point shown by the following explanation in q= 1. Since the standing wave of the tie point 1 has an antinode in the lattice plane, its absorption is larger than the mean absorption. For this reason, the standing wave decreases quickly as sz increases (anomalous absorption). On the other hand, since the standing wave of the tie point 2 has the node in the lattice plane, even when sz increases, it does not almost have absorption. Therefore, almost all X-rays penetrate the crystal(anomalous transmission). This result is the same as that of the conclusion by BC. However, the result of this paper is obtained by the dynamical diffraction only due to χ_{hi}, and is not the dynamical diffraction which contained χ_{hr} and χ_{hi} in χ_h, like SIA. Moreover, the studied result of this paper showed the following facts: the anomalous transmission (Borrmann effect) is produced by χ_{hi}, and it is not based on the synergistic effect of χ_{hr} and χ_{hi}. In $0<q$, the conclusion that the wave of the tie point 1 is carried out the anomalous absorption, and the wave of the tie point 2 is carried out the anomalous transmission, it is the same in the analysis of the Poynting vector and the standing wave. The analysis by the Poynting vector is convenient to examine the relationship between the dispersion surface and the energy flow, although the vector is averaged in minimum-space. On the other hand, since the analysis by the field intensity does not average minimum-space,

the information in the unit cell is obtained.

2.4. **Diffracted Wave and Transmitted Wave in Bragg case**

At present, the thickness dependability to the X-rays of the limited thick crystal is treated, and the diffracted intensity and the transmitted intensity using (2.83) are examined. And, the equation of the diffracted-intensity when the crystal thickness becomes semi-infinite was in agreement with FK's equation.

2.4.1 Rocking Curve

q, H, g, and δ are parameters like Laue case in examination of the rocking curve.

(i) **Dependence on q**

a) *In case of* $q = 0$

Fig.2.29 shows the rocking curve of the diffracted and the transmitted intensities for in s$H=\pi$. In this figure, dotted lines does not have absorption and thin solid lines have absorption. In case of $\chi_{oi} \neq 0$, g is set to -0.1 like Laue case. The rocking curve of the diffracted intensity without absorption is symmetry to $W = 0$, shows the maximum at $W = 0$, and has the pendellösung beat in $|W| > 1$.

Like the case where no absorption is, the rocking curve of the diffracted intensity with absorption is symmetrical with $W = 0$, shows the maximum at $W = 0$, and has a pendellösung beat in $|W| > 1$. The diffracted intensity with absorption is a little small as compared with the case where no absorption is. Although, the intensity of the node of the pendellösung beat without absorption is zero, the node with absorption is not zero. The rocking curve of the transmitted intensity without absorption is the minimum at $W = 0$, and it is symmetry to $W = 0$ and shows the pendellösung beat in $|W| > 1$.

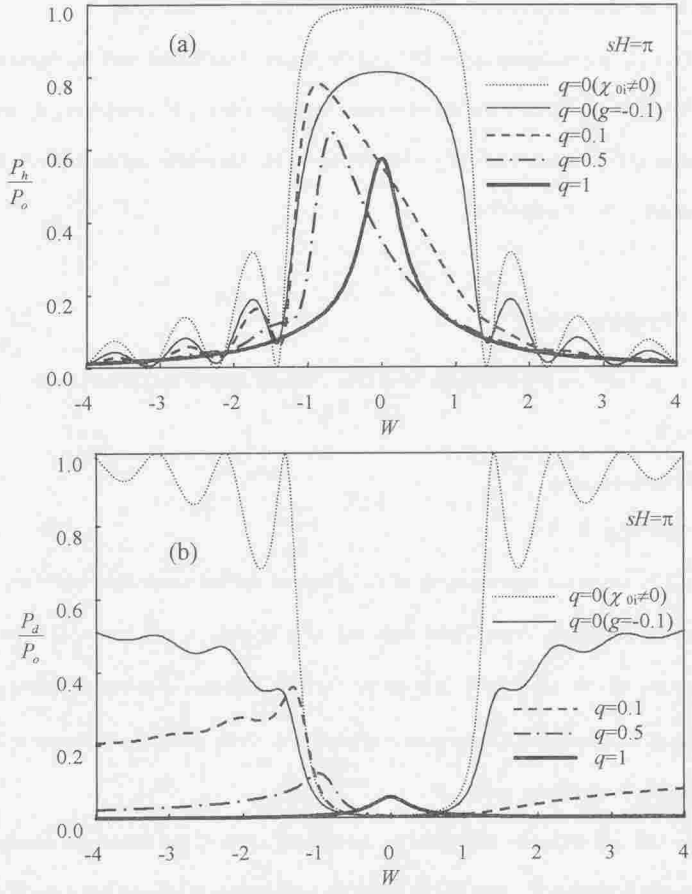

Fig.2.29 The rocking curves in the symmetric Bragg case for q= 0.0, 0.1, 0.5 and 1.0 when $sH=\pi$ and $\delta=0$.
(a)Diffracted waves. (b)Transmitted waves.

Although rocking curves of the transmitted intensity with absorption shows the change similar to rocking curves without absorption, the transmitted intensity wave is small. The diffracted and the transmitted intensities with absorption is shown in following equations

from (2.73) for q=0

$$\frac{P_h}{P_o} = \frac{\sin^2(sH\,\mathrm{Re}\sqrt{Q}) + \sinh^2(sH\,\mathrm{Im}\sqrt{Q})}{P_c}, \tag{2.129a}$$

$$\frac{P_d}{P_o} = \exp(-\mu_0 H') \cdot \frac{\left|\sqrt{Q}\right|^2}{P_c}. \tag{2.129b}$$

Where, there is the relationship of the following equation

$$P_c = \frac{1}{2}[(|\sqrt{Q}|^2 - W^2 - g^2)\cos(2sH\,\mathrm{Re}\sqrt{Q}) + (|\sqrt{Q}|^2 + W^2 + g^2)\cosh(2sH\,\mathrm{Im}\sqrt{Q})]$$
$$+ (g\,\mathrm{Re}\sqrt{Q} - W\,\mathrm{Im}\sqrt{Q})\sin(2sH\,\mathrm{Re}\sqrt{Q}) + (W\,\mathrm{Re}\sqrt{Q} + g\,\mathrm{Im}\sqrt{Q})\sinh(2sH\,\mathrm{Im}\sqrt{Q}), \tag{2.130a}$$

$$\mathrm{Re}\sqrt{Q} = \left[\frac{1}{2}(Q_r + |\sqrt{Q}|^2)\right]^{1/2}, \quad \mathrm{Im}\sqrt{Q} = \left[\frac{1}{2}(-Q_r + |\sqrt{Q}|^2)\right]^{1/2}, \tag{2.130b}$$

$$|\sqrt{Q}|^2 = [Q_r^2 + Q_i^2]^{1/2}, \quad (Q_r = W^2 - g^2 - 1,\ Q_i = 2gW). \tag{2.130c}$$

In this equation(2.130), there are the following conditions from the continuity of the complex plane

$$\begin{cases} \text{If}(Q_r \neq 0, Q_i > 0),\ \mathrm{Re}\sqrt{Q} \text{ and } \mathrm{Im}\sqrt{Q}, \\ \text{If}(Q_r > 0, Q_i < 0),\ \mathrm{Re}\sqrt{Q} \text{ and } -\mathrm{Im}\sqrt{Q}, \\ \text{If}(Q_r < 0, Q_i < 0),\ -\mathrm{Re}\sqrt{Q} \text{ and } \mathrm{Im}\sqrt{Q}. \end{cases} \tag{2.131}$$

If there is no absorption for (2.129 a), $\mathrm{Im}\sqrt{Q}$ is zero and the following equation will be obtained

$$\begin{cases} \dfrac{P_h}{P_o} = \dfrac{\sin^2(sH\sqrt{W^2-1})}{W^2 - 1 + \sin^2(sH\sqrt{W^2-1})}, & (|W| > 1) \\ \quad = \dfrac{\sinh^2(sH\sqrt{1-W^2})}{1 - W^2 + \sinh^2(sH\sqrt{1-W^2})}. & (|W| < 1) \end{cases} \tag{2.132}$$

This is the equations (3.143, 3.144) of Zachariasen [12] known well. In $|W| > 1$, the period of the pendellösung beat of the diffracted and the transmitted waves satisfy $sH\sqrt{W^2-1} = n\pi$

(n:integer).

b) *In case of* q=0.1 *and* q=0.5

When set to $q > 0$, rocking curves of the diffracted and the transmitted intensities is asymmetry to $W = 0$, and it very difference to compare at $q = 0$(see Fig.2.29). Since the asymmetry of this rocking curve is reversed to $W = 0$ when δ changes from 0 to π. Fig.2.29 shows the rocking curve for $\delta = 0$. The diffracted intensity for $q = 0.1$ becomes large gradually, when W changes from -4 to -1. The intensity becomes large rapidly at $W = -1$, and it shapes a peak. And, in $W > -1$, it becomes small gradually. The half value width of the rocking curve is smaller than that for $q = 0$. Although the pendellösung beat for $q = 0.1$ is visible to $W < -1$ side, the amplitude is smaller than that for $q = 0$. In $W > 1$ side, the beat does not look almost again.

On the other hand, the rocking curve of the transmitted intensity in $W < -1$ is larger than $W > 1$ side. And the intensity becomes large gradually as W approaches from the minus side to -1. The peak with the anomalous transmission is visible between $W = -2$ and -1, and its intensity became the minimum near at $W = 0$. While W increases in the plus side, the rocking curve becomes large gradually, and the pendellösung beat is visible to $W < -1$ side.

The rocking curve of the diffracted intensity for $q = 0.5$ becomes a little weaker than that $q = 0.1$. However, the tendency of change is the same as that for $q = 0.1$ almost. The half value width of the peak is narrower than $q = 0.1$, and the peak position carried out small movement at $W = 0$ side.

The rocking curve of the transmitted intensity becomes large gradually when W approaches from minus side to -1. The peak with the anomalous transmission is shaped $W \approx -1$. If W becomes large from $W = -1$, the rocking curve will become small abruptly. And the pendellösung beat is not seen. Rocking curves in $q = 0.1$ and 0.5 are examined in

detail in the section of the dispersion surface,

c) *In case of* q= 1

In q=1, the rocking curve (thick solid lines) of the diffracted and the transmitted intensities becomes symmetry like q= 0 to W= 0. Moreover, these rocking curves has the sharp peak at W= 0. This phenomenon greatly differs that for q= 0. The peak of the transmitted intensity is the anomalous transmission. If the crystal thickness is the same, the half value width of the peak for the diffracted and the transmitted intensities of Bragg case narrow to compared that of Laue case.

(ii) **Dependence on the crystal thickness**

In order to examine the dependence on thickness, let sH be the parameter like Laue case. The rocking curves of the diffracted and the transmitted intensities with sH in q= 0, 0.5 and 1 are shown Fig.2.30.

a) *In case of* q= 0

In the paragraph, the examination is the case when the absorption is not neglected, and is g = −0.1. When increase sH from $\pi/2$ to $3\pi/2$, the diffracted intensity at W= 0 also increase from 0.7 to 0.82. When sH becomes large, the minimum value of the transmitted intensity becomes small rapidly at W=0 and the bottom of the valley becomes flat.

When sH changes from 1, 2 to 3, the period of the pendellösung beat is set short to 1/2 and 1/3, and the amplitude of the beat becomes small.

b) *In case of* q= 0.5

The conditions of the examination are g_0 = −1 and δ = 0. In this case, the rocking curve of the diffracted and the transmitted intensities is asymmetrical, and the peak is always in the minus side of W. If sH increases, the peak becomes high and will become sharp in the

rocking curve of the diffracted intensity. The rocking curve of the transmitted intensity becomes weak according to the increase in *sH*, and the peak becomes sharp. The pendellösung beat is seen in the rocking curve of the diffracted intensity in the minus side of *W*. The period becomes short according to increase of *sH*.

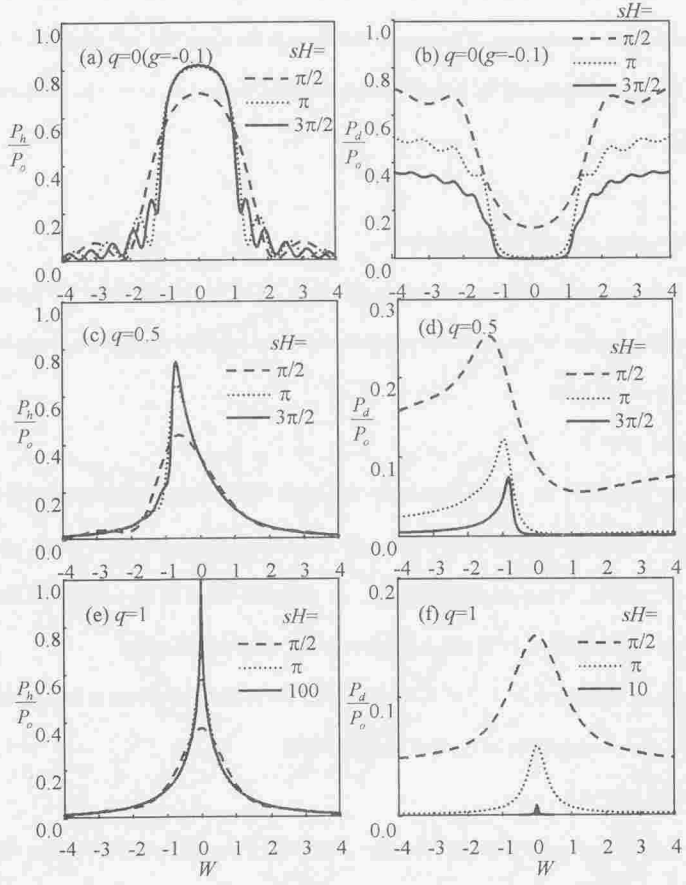

Fig.2.30 The rocking curves in the symmetric Bragg case for several *sH* when δ=0. (a)(c)(e);Diffracted waves. (b)(d)(f);Transmitted waves.

c) *In case of* q= 1

Here, g_0 = −1(See Fig.2.30 (e),(f)). Rocking curves of the diffracted intensity become sharp compared with the peak for q=0 at W=0, and become high incleasing the crystal thickness. In sH=100, the peak height is about 1. The rocking curve is in agreement with that the semi-infinite crystal[10] [17]. If the crystal becomes thick, although the rocking curve of the transmitted intensity will become small gradually, the peak becomes sharp at W=0. The pendellösung beat is not seen in this figure. However, if the crystal becomes the thickness equivalent to sH=1, the pendellösung beat will be looked at by the rocking curve of the diffracted and the transmitted intensities as shown in Fig.2.31.

The relationship among the diffracted intensity, the transmitted intensity and the crystal

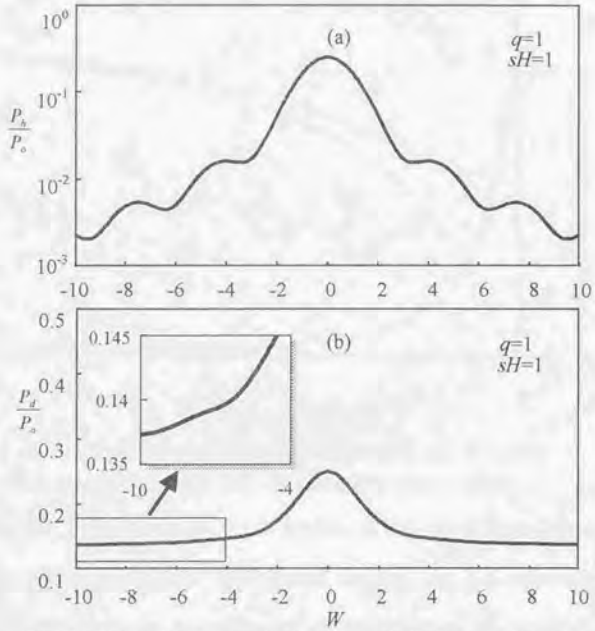

Fig 2.31 The rocking curves in the symmetric Bragg case for q=1.0 when sH=1 and δ=0. (a)Diffracted waves. (b)Transmitted waves.

thickness are examined in this paragraph for q=1. The diffracted and the transmitted intensities are shown by following equations at W= 0

$$\frac{P_h}{P_o} = \left(\frac{sH}{1+sH}\right)^2, \tag{2.133}$$

$$\frac{P_d}{P_o} = \left(\frac{1}{1+sH}\right)^2. \tag{2.134}$$

Consequently, total P is obtained by the following equation

$$P = \frac{1+sH^2}{(1+sH)^2}. \tag{2.135}$$

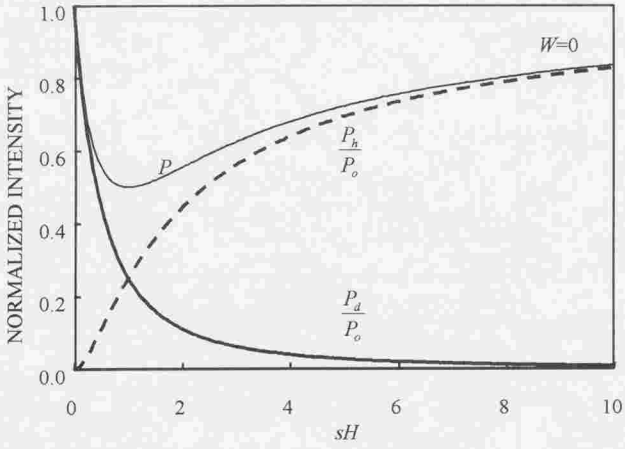

Fig 2.32 The change of the intensity with crystal thickness in the symmetric Bragg case for W=0 when q =1 and g_o=-1.0.

The result depend on sH of (2.133), (2.134) and (2.135) is shown in Fig2.32. To sH>6, the diffracted intensity(dashed line) becomes large quickly with increasing sH. After that, it approaches 1 slowly with increasing sH. On the other hand, the transmitted intensity will become small quickly. If sH becomes large, Intensity approaches 0 gradually after that.

These intensities are both 0.25 at sH=1.When sH increases from 0 to 1, total P becomes small gradually and shows the minimum value (0.5) at sH=1. After that, P becomes large gradually as the diffracted intensity with increasing sH, and approaches 1. The diffracted intensity which comes out from the upper surface of the crystal and the transmitted intensity which comes out from the under surface are equal at sH=1 by which the total P takes the minimum value. The condition of sH=1 shows the crystal thickness from which the absorption becomes the maximum.

d) *Semi-infinite crystal*

In the thick crystal (semi-infinite crystal), the reflection from the under surface of the crystal is neglected. Therefore, the diffracted wave is obtained the following equation only in consideration of one tie point in (2.83a)

$$\frac{P_h}{P_0} = (1-2p\sin\delta)\left|\frac{1}{\mathrm{W}+i\mathrm{g}'\pm\sqrt{\mathrm{Q}}}\right|^2 . \tag{2.136}$$

$\left|W+ig'\pm\sqrt{Q}\right|^2$ is as follows, when $\sqrt{Q}=\mathrm{Re}\sqrt{Q}+i\,\mathrm{Im}\sqrt{Q}$ and $\pm$ sign takes only a required term in (2.136), and it obtains the following deployment

$$\begin{aligned}\left|\mathrm{W}+i\mathrm{g}'\pm\sqrt{\mathrm{Q}}\right|^2 &= (A^2+B^2)^{1/2}+W^2+g'^2 \\ &\quad +\left\{[(A^2+B^2)^{1/2}+W^2+g'^2]^2-[(1-2q)^2+4p^2\cos^2\delta]\right\}^{1/2}, \\ &= [(1-2q)^2+4p^2\cos^2\delta]^{1/2}[\Pi+(\Pi^2-1)^{1/2}]. \end{aligned} \tag{2.137}$$

Where, there is the following relationship

$$\Pi = \frac{[(A^2+B^2)^{1/2}+W^2+g'^2]}{[(1-2q)^2+4p^2\cos^2\delta]^{1/2}}, \tag{2.138}$$

$$A = W^2-g'^2+2q-1, \tag{2.139}$$

$$B = 2(g'W-p\cos\delta). \tag{2.140}$$

After all, the diffracted intensity for the semi-infinite crystal in Bragg case is shown by

$$\frac{P_h}{P_o} = \kappa[\Pi - (\Pi^2 - 1)^{1/2}], \tag{2.141}$$

$$\kappa = \frac{(1 - 2p\sin\delta)}{[(1-2q)^2 + 4p^2\cos^2\delta]^{1/2}}. \tag{2.142}$$

This equation (2.141) is the same one as that of the equation (12) of FK [10]. If there is no absorption, since p=g'=0 for symmetric reflection, equation(2.141) is the same one as that of the equation (3.155) of Zachariasen[12], or the equation (19.76) of Miyake[1]. And the rocking curve obtained from equations under this condition shows top hat type. The equation (2.142) is applicable to the semi-infinite crystal. However, the equation (2.83) is applicable from the crystal with limited thickness to the semi-infinite crystal. Thus, the equation (2.83) is very convenience to the study of the dynamical diffraction with resonance scattering in Bragg case.

(iii) **Dependence on g (g_0)**

In sH=π, the rocking curves with the diffracted and the transmitted intensities which were obtained by changing in q and g are shown in the Fig.2.33. In q= 0, g changes from -0.10 to -0.13, and g_0 changes from -1.0 to -1.3 in $q \neq 0$. The rocking curve of the diffracted intensity becomes small gradually as increasing $|g|$ from 0.10 to 0.13(a). That of the transmitted intensity becomes small similarly.

In q = 0.5 and 1, when g_0 changes from −1.0 to −1.3, the rocking curve of the diffracted intensity will become small gradually. And the half value width of the peak becomes large. The tendency is the same also in the rocking curve of the transmitted intensity. If g_0 increases, the peak position on the rocking curve of the diffracted intensity will move to W= 0 side.

In q= 1, if $|g_0|$ increases, the rocking curve of the diffracted and the transmitted intensities will become small,. And, the half value width of the central peak becomes large gradually.

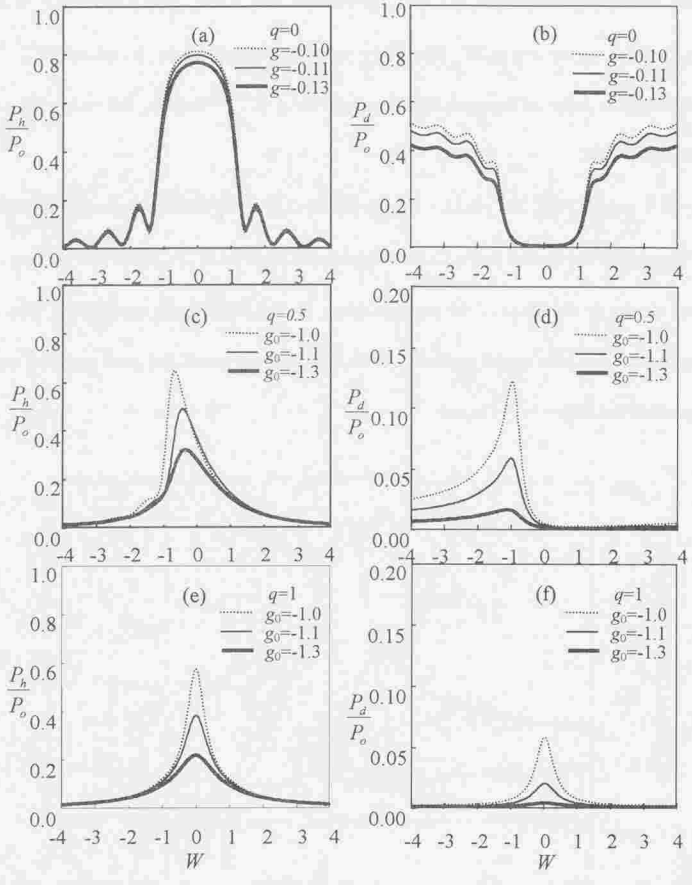

Fig.2.33 The rocking curves of diffracted and transmitted waves in the symmetric Bragg case for several g (g_0) when sH= π and δ=0. (a)(b)q=0;(c)(d)q=0.5;(e)(f)q=1.

(iv) **Dependence on phase difference δ**

In this section, the dependence on δ is examined like Laue case in Friedel pairs. In Laue case, when δ changed with 0 and π, the asymmetric reversal of the rocking curve appeared only in the transmitted intensity. In Bragg case, however, the rocking curves of the diffracted and the transmitted intensities are both asymmetry for $q \neq 0$. When δ takes 0 or π, the change reverse asymmetry to W. This effect has been carried out by Bucksch(1967) [18] in the diffracted intensity of the semi-infinite crystal for q<0.1. Therefore, the transmitted wave was not examined.

If q=0.5 and $sH=\pi/2$, the rocking curves of the diffracted and the transmitted intensities with changing δ are shown in Fig. 2.34. Asymmetric reversal in the diffracted rocking curve appears clearly as deviation of the peak position. On the other hand, asymmetric reversal in the transmitted rocking curve appears clearly as the deviation of the peak position and the difference of the intensity in the tail.

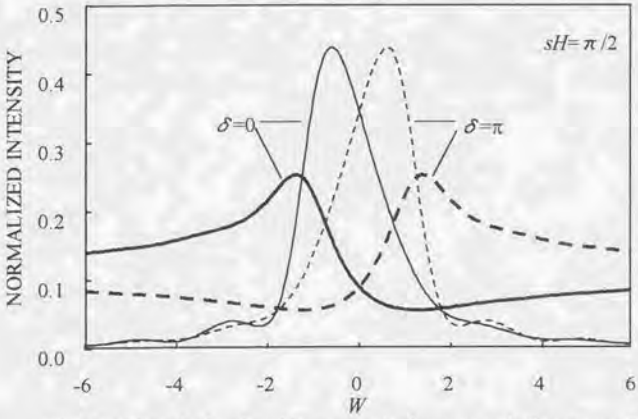

Fig.2.34 The calculated rocking curves in the symmetric Bragg case for q=0.5, g_0=-1 and $sH=\pi/2$. The thin solid and dashed lines are the curves of the diffracted beam, and the thick solid and dashed lines are the curves of the transmitted beam for δ =0 and $\delta=\pi$, respectively.

2.4.2. Dispersion Surface in Bragg Case

The examinations in the section are symmetrical Bragg case conditions. In the symmetric Bragg case, since $\beta = 0$, the equation of the complex dispersion surface is as follows from the real and the imaginary parts of (2.48), respectively

$$(X\cos\theta_B)^2 - (Y'\sin\theta_B)^2 + (Z'\sin\theta_B)^2 - \kappa_{oi}^{\ 2} = \frac{1}{4}\kappa_{or}^{\ 2}\overline{\chi_h}^2(1-2q), \qquad (2.143a)$$

$$Y'Z'\sin^2\theta_B + \kappa_{oi}X\cos\theta_B = -\frac{1}{4}\kappa_{or}^{\ 2}\overline{\chi_h}^2 p\cos\delta. \qquad (2.143b)$$

For the range of the q value is 0 to 1, if q<0.5, right-hand side of (2.143a) is positive. It is zero if q=0.5. And it is negative if q>0.5. Therefore, the dispersion surface is examined about each case of q = 0, 0.5 and 1.

(i) **In case of q=0**

Since p= 0, the following equation is obtained from (2.143)

$$(X\cos\theta_B)^2 - (Y'^2 - Z'^2)\sin^2\theta_B - \kappa_{0i}^{\ 2} = \frac{\kappa_{or}^{\ 2}|\chi_{hr}|^2}{4}, \qquad (2.144a)$$

$$Y'Z'\sin^2\theta_B + \kappa_{0i}X\cos\theta_B = 0. \qquad (2.144b)$$

This dispersion surface is shown in Fig.2.35(a, b) by the same simple displaying method as Fig.2.17 which considered by Laue case. (a) is g= 0 (without absorption), and (b) is g=–0.1 (with absorption). Solid lines express the real part of dispersion surfaces, and dashed lines express the imaginary part. In the dispersion surface (a) which is g= 0, Y'=Z'=0 at $|W|$=1. In the dispersion surface (b) which is g=–0.1, Y' and Z' are not zero at $|W|$=1. However, as following points are common to g=0 and g = –0.1: $|Y'|$ increases in 1<$|W|$, and $|Y'|$ is small in $|W|$<1, and $|Z'|$ shows tendency contrary to $|Y'|$.

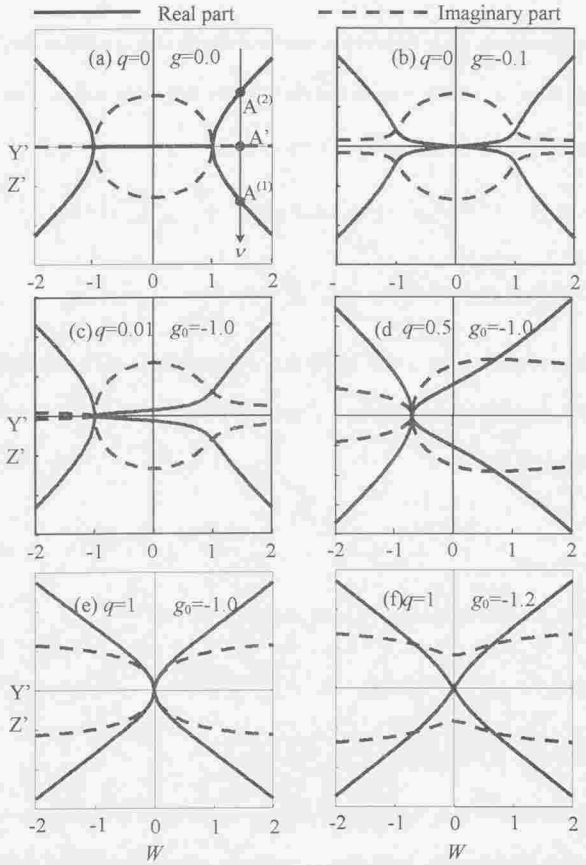

Fig.2.35. The dispersion surface in the symmetric Bragg case. The solid and the dashed lines are the real and the imaginary part of the curves. δ=0. (a) $q = 0$, $g = 0$. (b) $q = 0$, $g = -0.1$. (c) $q = 0.01$, $g_0 = -1.0$. (d) $q = 0.5$, $g_0 = -1.0$. (e) $q = 1$, $g_0 = -1.0$. (f) $q = 1$, $g_0 = -1.2$.

In g=0, the real part of the dispersion surface in $|W|>1$ shapes hyperbola in X-Y' plane, and, in $|W|<1$, the imaginary part shapes ellipse in X-Z' plane. The tie point is only one at $|W|=1$. However, in the case of $g = -0.1$, the tie point is in a point at $W = 0$, in all the other regions of W, there are two solutions in the real and the imaginary parts. In case of $g = 0$, since the

imaginary part in $|W|>1$ is 0, the node of the pendellösung beat of the diffracted intensity is 0, and the transmitted intensity is 1 when the node of the pendellösung beat of the diffracted intensity is 0.(dotted line in Fig.2.29). However, in case of $g = -0.1$, the imaginary solution is not zero. For this reason, since the wave from the under surface of the crystal becomes weak, the diffracted intensity is not zero in the node of the pendellösung beat of the diffracted wave(thin solid line in Fig.2.29).

(ii) **In case of q= 1**

In $g_0 = -1.0$, the following equation is obtained with the equation (2.143) for the dispersion surface

$$(Y'\sin\theta_B)^2 - (Z'\sin\theta_B)^2 - (X\cos\theta_B)^2 = 0, \qquad (2.145a)$$

$$Y'Z'\sin^2\theta_B = \frac{1}{2}\kappa_{or}|\chi_{hi}|X\cos\theta_B . \qquad (2.145b)$$

This equation satisfies $X=Y'=Z'=0$. And the complex dispersion surface of simple shape is shown in Fig.2.35(e). It differs in $q= 0$, if $|W|$ approaches zero, both $|Y'|$ and $|Z'|$ will approach zero remarkably. For this reason, the rocking curve of the diffracted and the transmitted intensities has the sharp peak in the center, as Fig.2.31(e),(f) showed. As shown in Fig.2.35(f), Y' for $g_0=-1.2$ shows the same change as $g = -1$. However, although $|Z'|$ shows the minimum value at $W= 0$, $|Z'|$ is not zero. For this reason, as Fig.2.33(e),(f) showed, the peak shape of $g_0= -1.2$ becomes broader than that of $g_0= -1$.

Two real parts of the dispersion surface exist for $q= 1$. Therefore, the pendellösung beat exists really as shown in Fig. 2.30.

(iii) **In case of q=0.01 and q=0.5**

Dispersion surfaces for q= 0.01 and q= 0.5 at δ =0 are shown in Fig.2.35(c),(d). In dispersion surfaces for q= 0 and q= 1, the real and the imaginary parts were symmetry to W=

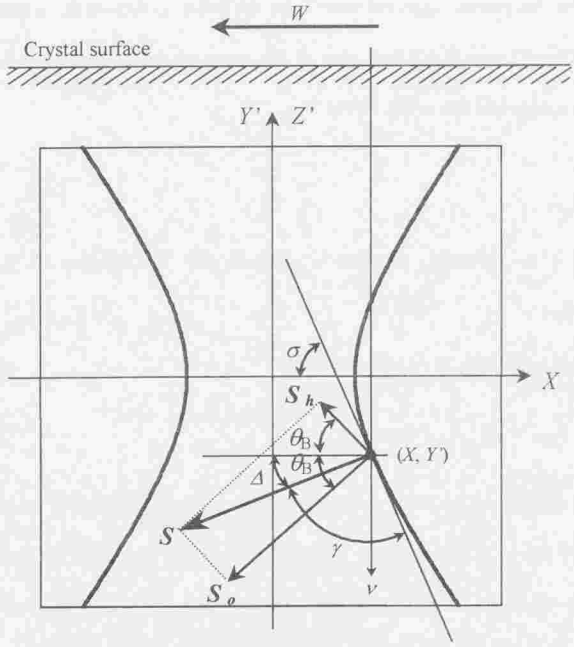

Fig.2.36 The relationship of the Poynting vector and the dispersion surface in the symmetric Bragg case when there is no absorption.

0. In (c) and (d), however, these dispersion surfaces are asymmetrical to W= 0. The dispersion surface for q= 0.01 is Y'=Z'=0 at $W \approx -1$, and the real part of the dispersion surface in W <1 is almost equal to that in case there is no absorption. Y' is not zero in W>−1 and Z' is also not zero in W<−1. On the other hand, although the real part of the dispersion surface at g_0= 0 (a) is zero at $|W|$= 1, in q= 0.01, both Y' and Z' not zero.

As the above description, the reason from which the intensity becomes the maximum at

near W=1 is understood from the shape of the dispersion surface in the diffracted and the transmitted intensities for q= 0.01 (see Fig.2.29). Therefore, behavior of rocking curves of the diffracted and the transmitted intensities for q=0.5 is explained from the characteristic of the dispersion surface like that for q= 0.01.

2.4.3. The Direction of Energy Flow

In this section, it is examined that the relationship between the real part of the dispersion surface and the direction of the Poynting vector $\boldsymbol{S}$ in symmetric Bragg case like Laue case. As shown in Fig.2.36, here, Δ is an angle between $\boldsymbol{S}$ and the diffraction lattice plane, and σ is the angle between the tangent in the tie point and axis X [19]. And it calculates the angle γ between the real part of the dispersion surface and the Poynting vector [20]. In symmetrical Bragg case, since β is zero, the following relationship is obtained

$$\sin\theta_1 = \sin\theta_2 = \cos\theta_B , \tag{2.146a}$$

$$\cos\theta_1 = -\cos\theta_2 = \sin\theta_B . \tag{2.146b}$$

Differentiating (2.143a) with respect to X, and the following equation is obtained

$$X\cos^2\theta_B - (Y'\frac{dY'}{dX} - Z'\frac{dZ'}{dX})\sin^2\theta_B = 0 . \tag{2.147}$$

The following equation is obtained from a equation (2.143b)

$$(Y'\frac{dZ'}{dX} + Z'\frac{dY'}{dX})\sin^2\theta_B + \kappa_{0i}\cos\theta_B = 0 . \tag{2.148}$$

$\frac{dZ'}{dX}$ is obtained from the equation (2.147) and substitutes the result to (2.148). And the following equation is obtained from $dY'/dX = \tan\sigma$

$$\tan\sigma = \frac{XY'\cos\theta_B - Z'\kappa_{0i}}{(Y'^2+Z'^2)\sin\theta_B}\cot\theta_B . \tag{2.149}$$

Moreover, the following relationship is obtained from Fig.2.37 for symmetric reflection

$$\frac{\sin(\theta_B+\Delta)}{\sin(\theta_B-\Delta)} = \frac{|D_h^{(j)}|^2}{|D_o^{(j)}|^2} . \tag{2.150}$$

Here, j is the number of the tie point. The following relationship is obtained from this equation

$$\tan\Delta = \frac{|R^{(j)}|^2-1}{|R^{(j)}|^2+1}\tan\theta_B . \tag{2.151}$$

Consequently, tanγ by the angle between the real part of the dispersion surface and the Poynting vector $\boldsymbol{S}$ is given by

$$\tan\gamma = \tan(\Delta+\sigma) . \tag{2.152}$$

When changing q from 0 to 1, γ is shown in Fig.2.37.

In q= 0 without absorption, the Poynting vectors are directed along the normal to the hyperbola. This result is the same as that of the proof of Kato [15] and Hung[19]. However, the real part of the dispersion surface is set to Y=0 in $|W|$<1. The real part of the dispersion surface and the Poynting vector are parallel in the place without intersect perpendicular.

That is, in this total-reflection region, the direction of the Poynting vector is parallel to the lattice plane, and there is no inconsistency in this conclusion. γ approaches 90° gradually as χ_{hi} component increases in $|W|$<1, when there is absorption. And, in q= 1, the deviation of γ from 90° is the smallest.

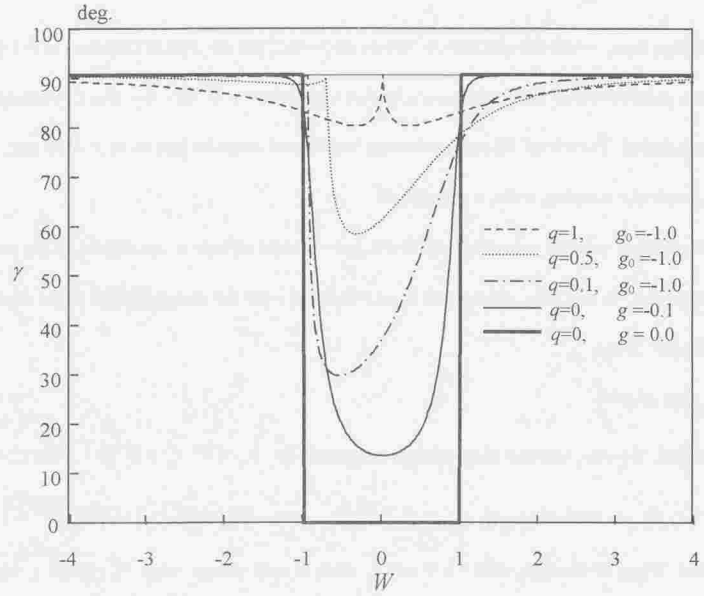

Fig.2.37 The variation of γ with respect to W for different values of q in the symmetric Bragg case.

2.4.4. Wave Field in Crystal

In Bragg case, when the absorption cannot neglected, unless crystal thickness is the very thin, the observation of the pendellösung beat is impossible. It is very few that this condition can be satisfied. Therefore, The pendellösung beat do not consider just to more than this, but we examine the standing wave in the crystal.

The standing wave is examined under the symmetrical reflective conditions in the semi-infinite crystal. In this case, since there is no reflection from the under surface of the crystal, the tie point is one.

(i) **In case of q= 0**

The first, the case without absorption is examined. In $\chi_{oi} = 0$, $Q = W^2 - 1$ from (2.44). Since $\overline{\chi_h}/\chi_{-h} = \exp(\mathrm{i}\,\alpha_{hr})$, if $\alpha_{hr} = \pi$, $\overline{\chi_h}/\chi_{-h} = -1$. Therefore $R = W + \sqrt{W^2 - 1}$ is obtained. When W changes with −1, 0 and 1, since R may change with −1, −i and 1, phase difference Ω of the standing wave changes with $-\pi$, $-\pi/2$ and 0. This relationship is shown in the right side of the upper row of Table 2.2.

The standing wave at W= 0 is shown in the following equation using (2.92)

$$I(x) = |D(x)|^2_{(W=0)} = \frac{|E_0|^2}{2} \exp(-2sz\,\mathrm{Im}\sqrt{Q})[1 + \sin(2\pi\frac{x}{d})]. \qquad (2.153)$$

Coordinates x is the same direction as reciprocal-lattice vector $\boldsymbol{h}$. The inside of [ ] in (2.153) shows the standing wave which has lattice interval d in the period. Standing waves of q= 0 and q= 1 are shown in Fig.2.38, when W=−1,0 and 1. In q= 0, the node of the standing wave is on the lattice plane at W=−1, and the antinode of the standing wave is on the lattice plane at W= 1.

As shown in Fig.2.26(b), field intensities $I(x)$ of four surfaces at x= 0, d/4, d/2 and 3d/4 are calculated in between lattices, and behaviors of the field intensity are examined.

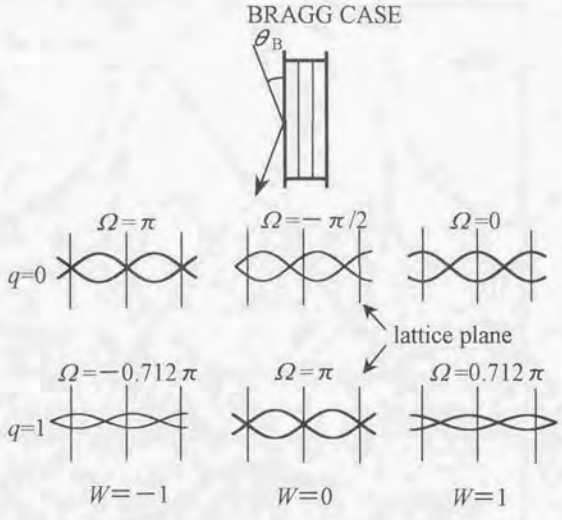

Fig.2.38 Standing waves in the Bragg case. The upper figures for q=0 and the lower for q=1.

The result for E_0= 1 is shown in Fig.2.39. In Bragg case, the plane at x= 0 contains the origin of the unit cell. (a) is g= 0 and (b) g=-0.1. On the surface(x= 0) at g= 0, since the inside of [ ] in (2.153) is 1+W, when W changes from −1, 0 to 1, the field intensity increases linearly from 0, 2 to 4. On the other hand, the change in the center (d/2) is contrary to x= 0. In x=d/4, $I(x)$ is 0 at W= 0, and $I(x)$ is 4 at x=3d/4. When there is absorption for q= 0, $I(x)$ is shown in Fig.2.39(b). The behavior shows the same change as no absorption(a).

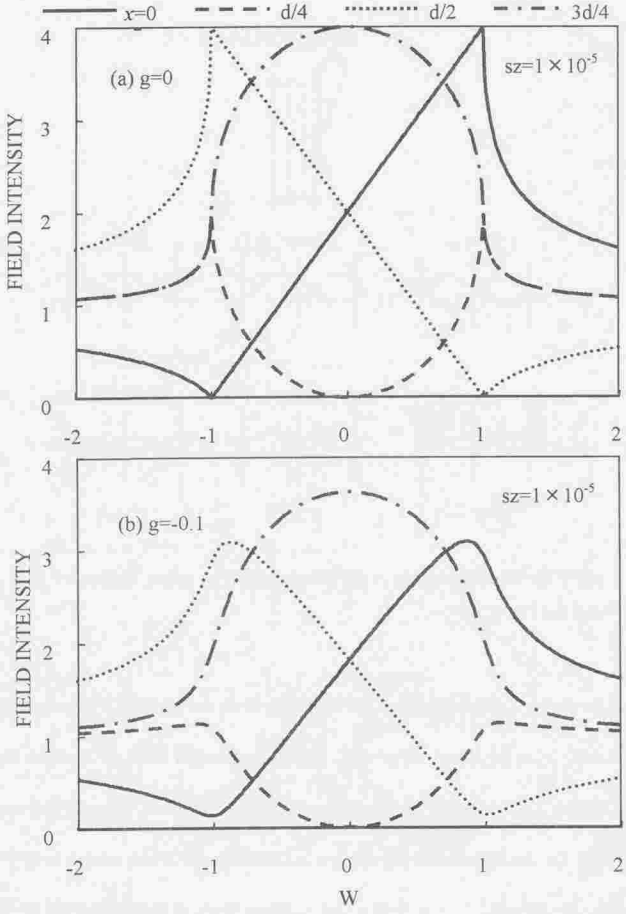

Fig.2.39 The change of the wave field $I(x)$ for x=0, d/4, d/2 and 3d/4 in the symmetric Bragg case for q=0 and $\alpha_{hr}=\pi$. (a)g=0. (b)g=-0.1.

(ii) **In case of q= 1**

Phase Ω of the standing wave for q= 1 is shown in the right side of the lower row Table.2.2. When W changes with −1, 0 and 1, Ω changes with −0.712 π, π and 0.712 π.

The calculated result about $I(x)$ is shown in Fig.2.40. Here, $\alpha_{hi} = \pi$. In the lattice plane at x= 0, since the standing wave is the node in this case, $I(0)$=0 at W= 0. On the other hand, $I(d/2)$ in middle takes the minimum value at W= 0. When W changes with –1, 0 and 1, $I(d/4)$ at x= $d/4$ decreases sharply from large value to small value at W= 0. Moreover, $I(3d/4)$ shows the change with reverse $I(d/4)$ to W= 0. That is, $I(3d/4,W) = I(d/4, -W)$. In q= 0, the standing wave at W= 0 was not able to have an antinode or a node in the crystal surface or the center between lattices, respectively. However, the standing wave for q= 1 has the node in the crystal surface, and has the antinode in the center between lattices.

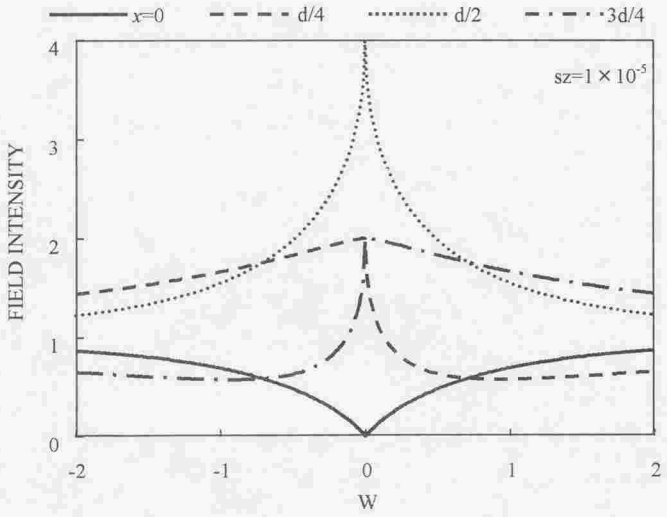

Fig.2.40 The change of the wave field for x=0, $d/4$, $d/2$ and $3d/4$ in the symmetric Bragg casefor q=1 and α_{hi}= π.

Conventionally, behavior of the X-ray standing wave was investigated from observation of secondary radiation, such as fluorescence X-rays and secondary electron. And, the

position of the impurities atom or the adsorption atom in the crystal surface etc. has been determined. Although these studies by the standing-wave method have been performed by it $q \ll 1$ in Bragg case, if we use the phase change of the standing wave to $q = 0$ to 1, probably, the field of the study will be expanded.

Table 2-2. The phase factor Ω for W=-1,0 and 1. The upper column for q=0 and the lower for q=1. The values of -0.712π and 0.712π are numerically obtained.

		Symmetric Laue case			Symmetric Bragg case (semi-infinite)		
	tie point	$W=-1$	0	1	$W=-1$	0	1
q=0	1	0	0	0	$-\pi$	$-\pi/2$	0
$\alpha_{hr}=\pi$	2	π	π	π			
q=1	1	$-\pi/2$	0	$\pi/2$	$-0.712\,\pi$	π	$0.712\,\pi$
$\alpha_{hi}=\pi$	2	$-\pi/2$	π	$\pi/2$			

Table 2-3. The damping factor of the wave field given by eq.(2.92) at $W=-1$, 0 and 1 for two tie points in the symmetric Laue case.

q=1	Change of term $\exp(4\pi k_{ozi}^{(i)} z)$ for symmetric Laue case		
tei point	$W=-1$	$W=0$	$W=1$
1	$\exp(-\mu z/\cos\theta_B)$	$\exp(-2\mu z/\cos\theta_B)$	$\exp(-\mu z/\cos\theta_B)$
2	$\exp(-\mu z/\cos\theta_B)$	1	$\exp(-\mu z/\cos\theta_B)$

APPENDIX A: **Relationship among *W*, Incident Angle α and Glancing Angle α_0.**

In symmetrical reflection, supposing α_{0L} is the glancing Angle in Bragg condition, following formulae are satisfied in Laue case

$$\alpha_0 = \frac{\pi}{2} - \alpha, \ \alpha_{0L} = \frac{\pi}{2} - \theta_B. \tag{a1}$$

Therefore

$$\Delta\theta = \theta_B - \alpha. \tag{a2}$$

The following conditions are satisfied in Bragg case

$$\alpha_{0L} = \theta_B. \tag{a3}$$

Therefore

$$\Delta\theta = \alpha_0 - \theta_B. \tag{a4}$$

In Bragg case, $\Delta\theta$ neglects the refractive index. α and α_0 of Laue case and Bragg case are shown in the following figure.

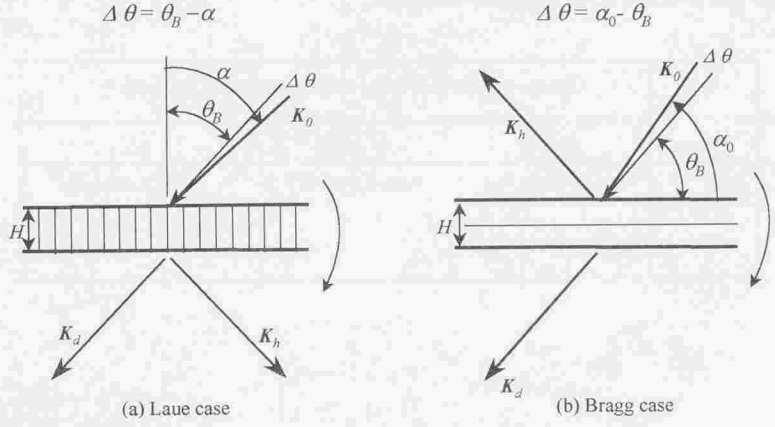

APPENDIX B: **Energy Flow of Electromagnetic Field**

Generally, the energy flow in a electromagnetic field is expressed as follows as a Poynting vector

$$\boldsymbol{S} = \frac{c}{4\pi}(\boldsymbol{E} \times \boldsymbol{H}^*) . \tag{b1}$$

Where, * is the complex conjugate. The $\boldsymbol{S}$ is energy which passes unit time and unit area through a surface perpendicular to $\boldsymbol{E}$ and $\boldsymbol{H}$ (density of energy flow). Since almost all ε is 1, a equation (b1) is as follows

$$\boldsymbol{S} = \frac{c}{4\pi}(\boldsymbol{D} \times \boldsymbol{H}^*) . \tag{b2}$$

Since both time change and periodic space change are contained in $\boldsymbol{D}$ and $\boldsymbol{H}$, generally, these sets as follows

$$\boldsymbol{D} = \exp(2\pi i \nu t) \sum_h \boldsymbol{D}_h \exp[-2\pi i(\boldsymbol{k}_h \cdot \boldsymbol{r})] , \tag{b3}$$

$$\boldsymbol{H} = \exp(2\pi i \nu t) \sum_h \boldsymbol{H}_h \exp[-2\pi i(\boldsymbol{k}_h \cdot \boldsymbol{r})] . \tag{b4}$$

A time average of $\boldsymbol{S}$ is as follows by using these $\boldsymbol{D}$ and $\boldsymbol{H}$

$$\overline{\boldsymbol{S}} = \frac{c}{8\pi} \mathrm{Re}(\boldsymbol{D} \times \boldsymbol{H}^*) . \tag{b5}$$

The following related formulae are known in vector analysis

$$K_0 \boldsymbol{D}_h^* = \boldsymbol{H}_h^* \times \boldsymbol{k}_h \tag{b6}$$

$$\begin{aligned} K_0(\boldsymbol{k}_h \times \boldsymbol{D}_h^*) &= \boldsymbol{k}_h \times (\boldsymbol{H}_h^* \times \boldsymbol{k}_h) \\ &= k_h^2 \boldsymbol{H}_h^* \end{aligned} \tag{b7}$$

By using (b6), (b7) and $\boldsymbol{k}_h \perp \boldsymbol{H}_h$, (b5) will become as follows

$$\overline{\boldsymbol{S}} = \frac{c}{8\pi} \mathrm{Re} \sum_h \sum_{h'} \frac{1}{|\boldsymbol{k}_{h'}|} (\boldsymbol{D}_h \times (\boldsymbol{k}_{h'} \times \boldsymbol{D}_{h'}^*)) \exp[2\pi i(\boldsymbol{k}_{h'} - \boldsymbol{k}_h) \cdot \boldsymbol{r}] . \tag{b8}$$

Since the real part of the term of $(\boldsymbol{k}_{h'} - \boldsymbol{k}_h) \cdot \boldsymbol{r}\ (h \neq h')$ corresponds to the lattice period of the wave field in a crystal, if it takes a space average in the range of a dynamical diffraction, it will become zero. However, since the imaginary part remains, it sets with $\boldsymbol{k}_{oi} \cdot \boldsymbol{r}$. If h' and h after the space average are placed with h, (b8) is as follows in consideration of $\boldsymbol{k}_h \perp \boldsymbol{D}_h$

$$\overline{\overline{\boldsymbol{S}}} = \frac{c}{8\pi} \exp[4\pi(\boldsymbol{k}_{oi} \cdot \boldsymbol{r})] \sum_h \frac{\boldsymbol{k}_h}{|\boldsymbol{k}_h|} |\boldsymbol{D}_h|^2 . \qquad \text{(b9)}$$

In two- wave approximation, since only the diffracted wave and the transmitted wave are examined, (b9) becomes a equation (2.88).

References

[1] S. Miyake(1969)"*X-ray Diffraction*".Tokyo:Asakura(in Japanese).

[2] G. Molière(1939)"*Quantenmechanische Theorie der Röntgenstrahlinterferenzen in Kristallen*", *Ann. Phys.*, **35**, 272-296, 297-313.

[3] R. W. James(1954)"*The Optical Principles of the Diffraction of X-Rays*", G.Bell and Sons.

[4]P. P. Ewald(1913)"*Zur Theorie der Interferenzen der Röntgenstrahlen in Kristallen*", Phys. Soc., 14, 465-472.

[5] B. W. Batterman, & H. Cole (1964)"*Dynamical Diffraction of X-rays by Perfect Crystals*", *Rev. Mod. Phys.*, **36**, 681-717.

[6] Z. G. Pinsker(1978)"*Dynamical Scattering of X-Rays in Crystals*", Berlin Springer.

[7] T. Fukamachi, R. Negishi and T. Kawamura(1995)"*The Dispersion Surface of X-rays Very Near the Absorption Edge*", *Acta Cryst.***A51**,253-258.

[8] M. Kuriyama, K. Takumi, T. Knamaru, H. Katoh and K. Ishida(1997)"*X-Ray Dispertion Corrections Obtained by Rocking Curve Measurements for Ge and*

[9] Z. Xu, Z. Zhao, C. Guo, S. Zhou, T. Fukamachi, R. Negishi and T. Nakajima(1995) "*Bragg reflection and transmission of x-rays induced by the imaginary part of the atomic scattering factor*". *J. Phys., Condensed. Matter* 7, 8089-8098.

[10] T. Fukamachi and T. Kawamura(1993)"*Xray Diffraction when the Real Part of the Scattering Factor is Zero*", *Acta Cryst.*, A**49**, 384-388.

[11] V. M. Laue(1952)"*Die Energieströmung bei Röntgenstrahl-Interferenzen in Kristallen*", *Acta Cryst.***5**,619-625.

[12] W. H. Zachariasen(1945)"*Theory of X-Ray Diffraction in Crystals*",Dover,New York.

[13] T. Fukamachi, R. Negishi and T. Kawamura(1994)"*Dynamical Diffraction in the Laue Case with Borrmann Absorption*", *Acta Cryst.*, A**50**, 475-480.

[14] Z.Xu, Z. Zhao and C. Guo(1996)"*The relationship of Poyntig vector and the dispersion surface in the absorbing crystal*", *J. Phys.:Condens. Matter* **8**,5977-5985.

[15] N. Kato(1958)"*The Flow of X-rays and Material Waves in Idealy Perfect Crystals*". *Acta Cryst.***11**,885-887.

[16] P. P. Ewald(1958)"*Group Velocity and Phase Velocity in X-ray Crystal Optics*", *Acta Cryst.*, **11**, 888-891.

[17] N. Kato(1992)"*A Note on the Darwin-Prins Rocking Curve for Perfect Crystals*",

Acta.Cryst., **A48**,829-833.

[18] V. R. Bucksch, , J. Otto. and M. Renninger(1967)"*Die 'Diffraction Pattern' des Idealkristalls für Röntgenstrahlinterferenzen im Bragg-Fall*", *Acta Cryst.* **23**, 507-511.

[19] H. H. Hung(1993)"*Relation of the Pointing vector normal to the dispersion surface*", *Acta Cryst.***A49**, 793-794.

[20] Z. Xu, C. Guo, Z. Zhao, T. Fukamachi and R. Negishi(1997)"*The Relationship Between the Poynting vector and the Dispersion Surface in the Bragg Case*", *J. Phys.:Condens. Matter*., L275-278.

CHAPTER III EXPERIMENTAL

In this Chapter, several simulations and experiments performed by the author are described. In GaAs200 reflection, the Fourier coefficient of the electric susceptibility near Ga K-absorption edge is numerically calculated. It was found in the simulation that the phase difference δ changes from 0, π, 0 to $-\pi$ as a function of X-ray energy across Ga and As *K*-absorption edges. The simulated result is verified by the following four experiments: (1)the observed rocking curves in Laue case, (2)the intensity changes of the fluorescence X-rays depending on the incident X-ray energy, (3)the observed rocking curves below Ga K-absorption edge for GaAs200 in Laue case as well as for (4) GaAs600 in Bragg case. In topographic observation when the resonance scattering is strong in GaAs 200, the contrast has been remarkably improved compared with that of weak absorption. Rocking curves in Laue case are observed, and anomalous-scattering factors were determined by using a profile fitting method.

3.1 Dynamical Diffraction due to $\chi_{hr}=0$ in Simple Substance

When the theoretical value of PH is used(see Chpter I_1.4.1), the real part $f^0_{Ge}+f'_{Ge}$ of the atomic scattering factor of germanium by the isolated atom became zero from *K*-absorption edge of germanium in $\pm$1.3eV, moreover, in during the period in Fig.1.6(b), it is minus. The phase of χ_{hr} in this case is 0 or π. If the phase in the case of plus value is 0, the phase in the case of minus value is π.

In actual germanium crystal, the integrated reflection intensities(IRIs) of Ge 844 in Bragg case which it measured near the Ge *K*-absorption edge is shown in Fig.3.1[1]. The integrated reflection intensities becomes small gradually when the energy approaches from -8eV to the

absorption edge. And in -2.8eV, IRIs becomes the minimum, and it will become large if the energy approaches the absorption edge further. A dotted line shows the integrating reflecting powers(IRPs) which are calculated by using SIA's equations, and a solid line shows the result which are calculated using the theory of this paper. A dotted line becomes zero at ±1.3eV. Since there is the diffraction only due to f'', even when $f^0_{Ge}+f'_{Ge}$ is zero (the minimum value is shown). There is no sharp valley which the open circles shows in the measurement result by the actual crystal.

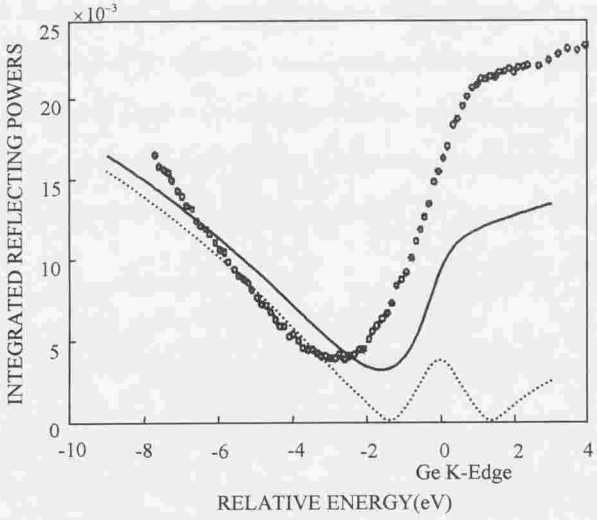

Fig.3.1 The calculated IRPs in atomic units (solid line) and the measured IRIs in arbitrary units (open circles) of the Ge 844 reflection near the K-absorption edge in the symmetric Bragg case. The measured IRIs are scaled so that the minimum intensity is the same as the calculated one.

The above conclusion is applied also to Fig.1.7. In Laue case, the shoulder structure seen below of the *K*-absorption edge corresponds to the condition $f^0_{Ge}+f'_{Ge}=0$ from the measurement of integrated reflecting powers of Ge 844. The position from the *K*-absorption

edge is -1.3eV in theoretical calculation, and measured value is -2.8eV. Moreover, according to calculation of SIA's equation, at −1.3eV, the integrated reflecting powers of Laue case and Bragg case are zero. However, the present IRPs becomes to the valley in the Bragg case, it is not zero at −1.3eV which the dynamical diffraction only due to f'' produces. By experiment, existence of the dynamical diffraction only due to f'' accepted by -2.8eV from *K*-absorption edge.

If rocking curve is measured precisely around -2.8eV from the *K*-absorption edge, the sign of $f^0 + f'$ will be determined from the reversal of asymmetry in the rocking curve. Because in a monatomic single atom crystal like germanium, f'' is always positive, χ_{hi} is always negative and α_{hi} is π.

3.2 χ_{hr} and χ_{hi} for GaAs 200 near Ga and As *K*-Absorption Edges

Although GaAs is a polar crystal, 200 reflection does not show polarity. That is, 200 and $\bar{2}00$ are a Friedel pair. In this case, δ is either 0 or π. The calculated result of χ_{hr} and χ_{hi} for GaAs 200 near Ga and As *K*-absorption edges are shown in Fig.3.2[2]. Here, the origin of the unit cell is taken as a Ga atomic site. In this figure, region(1) is lower energy region from Ga *K*-absorption edge. Region(2) is higher than the edge where χ_{hr} is positive. Region (3) is still higher than Ga *K*-absorption edge and χ_{hr} below As *K*-absorption edge where χ_{hr} is negative. And region (4) is higher than As *K*-absorption edge. Phase difference δ changes from region (1) to (4) as follows.

(1) $\chi_{hr}>0$, $\chi_{hi}>0$, $\delta=0$,

(2) $\chi_{hr}>0$, $\chi_{hi}<0$, $\delta=\pi$,

(3) $\chi_{hr}<0$, $\chi_{hi}<0$, $\delta=0$, (3.1)

(4) $\chi_{hr}<0$, $\chi_{hi}>0$, $\delta=-\pi$.

At the boundary of (1) and (2), $\chi_{hi}=0$ and only χ_{hr} is not zero($q=0$). At the boundary of

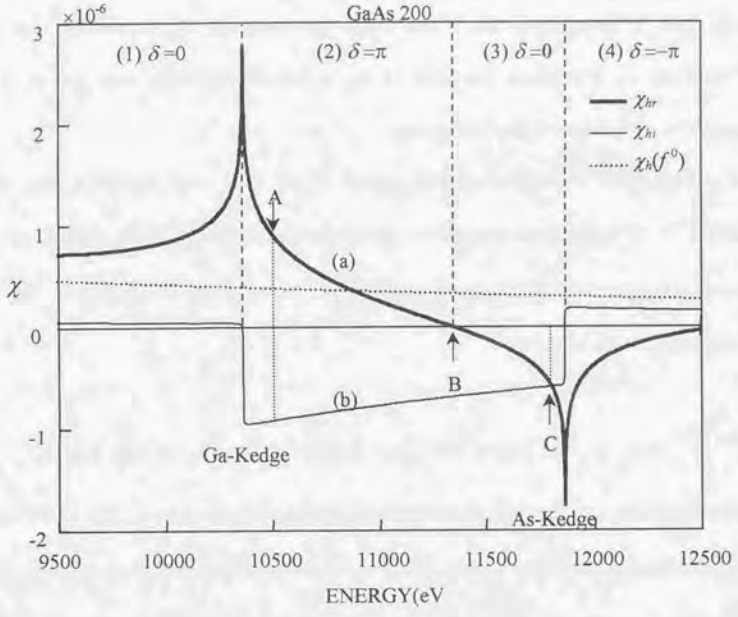

Fig.3.2 χ_{hr} and χ_{hi} for GaAs 200 near Ga and As K-absorption edges.
The dotted line is χ_h without resonance(anomalous) scattering factor.

(2) and (3), $\chi_{hr}=0$ and only χ_{hi} is not zero($q=1$, arrow B). At the positions indicated by arrows A and C in Fig.3.2,the following conditions are satisfied

At A, $\chi_{hr}=-\chi_{hi}$, ($q=0.5$, $\delta=\pi$), (3.2a)

At C, $-\chi_{hr}=-\chi_{hi}$, ($q=0.5$, $\delta=0$). (3.2b)

Since GaAs has the zinc-blende structure, the crystal structure factor F of 200 is described in

the following form

$$F = 4\left[(f_{Ga}^{0} + f_{Ga}^{'} + if_{Ga}^{''}) - (f_{As}^{0} + f_{As}^{'} + if_{As}^{''})\right] \quad (3.3)$$

Atomic numbers of Ga and As are 31 and 33, respectively, and they are close to each other. As the difference of f_{Ga}^{0} and f_{As}^{0} is small, the resonance scattering of Ga appears remarkably in Ga *K*-absorption edge, and the resonance scattering of As appears remarkably in As *K*-absorption edge. As shown in Fig.3.2, χ_{hr} and χ_{hi} change remarkably in the energy range around Ga and As *K*-absorption edges. For this reason, GaAs 200 is very convenient for the study of the dynamical diffraction with the X-ray resonance scattering. The experimental results are described the rocking curve near Ga and As K-absorption edges for GaAs 200.

3.3 **Experimental System and Specimen**

3.3.1 Experimental System

The experiment was carried out at BL6C1, KEK-PF. An example of the experimental equipment is shown in Fig.3.3. SR X-ray is monochromized by a double crystal monochromator of + −arrangement of Si 111. The monochromatic X-rays passed two ion-

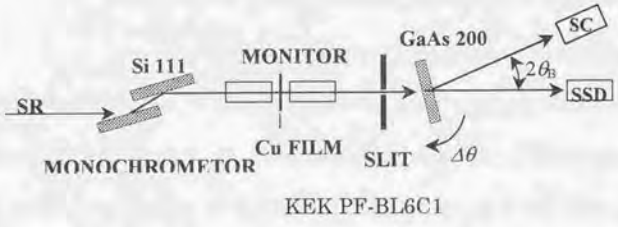

Fig.3.3 Schematic diagram of the experimental set up.

chambers which are used as a monitor of the incident beam, and enter the sample crystal. These monitors were used for the energy calibration by observing XANES of Cu *K*-absorption edge. The diffracted beam and the transmitted beam were detected by a scintillation counter(SC) or a solid-state detector(SSD) with pure germanium type.

3.3.2 Specimen

The specimen crystal is a single crystal of GaAs with low Si doped. The EPD value of this GaAs is less than 500 cm^{-2}. Yoshizawa et al.[3] observed an X-ray resonance scattering pendellösung beat by using this specimen of GaAs. Since the GaAs specimen is such a perfect crystal that it can be used for the study of the dynamical diffraction. The parallel plate of 10×10mm was cut down from the wafer of GaAs with a diameter of 1 inch, and was mechanical polished to be about 150μm in thickness. Then, the damage layer by the mechanical polish was removed by chemical etching. The thickness of the specimen is 134μm.

3.4 **Measurement of Rocking curves**

3.4.1 Observation of δ and Dynamical Diffraction for $q \geq 0.5$

(i) Measured rocking curves for GaAs 200

The influence of δ in the rocking curve was examined of the transmitted beam in Laue case in Chapter II (2.3.1.iv). When q= 0.5 and $\delta = 0$, the rocking curve of the transmitted beam has a peak due to the anomalous transmission in the negative side of W as shown in Fig.2.6(b). And the intensity of the tail in the negative side is higher than the tail in the positive side. On the other hand, for $\delta = \pi$, the peak position and the height of the tail are

both reversed. Measured rocking curves of the diffracted and the transmitted intensities are shown by Fig.3.4. The thin solid line is the diffracted intensity and the thick solid line is the transmitted intensity. In (a), X-ray energy is at the position of arrow A in Fig.3.2., and in (c) it is at the position of arrow C. The value of q is expected to be 0.5 at the positions of A and C. The curve (a) shows the tendency for $\delta = \pi$ and (c) shows the tendency for $\delta = 0$. Thus, δ is determined. And the diffraction only due to χ_{hi} is expected at the energy indicated by arrow B in Fig.3.2. Fig.3.4(b) is the experimental result of the rocking curve at the energy of B in Fig.3.2. In this case, the q value is q=1, and the rocking curves of the diffracted beam and the transmitted beam are symmetric with respect to W= 0. Then, the peak positions should be same. In Fig.3.4(b), the positions of the two peaks are almost the same. However, the tail heights in the rocking curve of the transmitted intensity are not the same in the left hand side(for $-|W|$) and right hand side(for $+|W|$). According to theory, the tail heights in the left hand side and the right hand side should be the same when q=1. The origin of the difference between the theory and the experiment is attributed to be that the energy position of B predicted in theory, is slightly different. However, the asymmetry of the rocking curve in (b) is far less than that seen in (a) or (c). Therefore, from this experimental result, it can be concluded that the condition of q= 1 should be obtained not far from the point B.

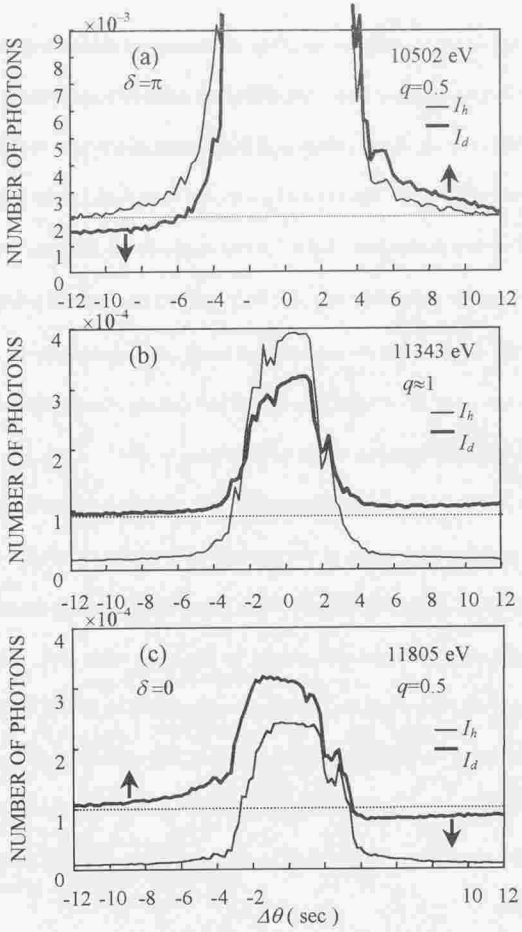

Fig.3.4 The measured rocking curves for GaAs 200. (a)at point A , (b)at point B and (c) at point C in Fig.3.2. The thick lines are the curve of the transmitted beam and the thin lines that of the diffracted beam.

(ii) **Yield curves of fluorescence X-rays**

a) *Experiment*

The yield intensity of fluorescence X-rays was measured by using the experimental setup shown in Fig.3.5. The experiment was carried out under the condition of symmetric Laue case for GaAs 200[4]. Diffracted X-rays from a crystal are detected by SSD, and fluorescence X-rays in the entrance side and the exit side were detected by SCs. The experimental results of the rocking curve of fluorescence X-rays and the diffracted intensity are shown in Fig.3.6. The rocking curve of the diffracted beam is shown only at the X-ray

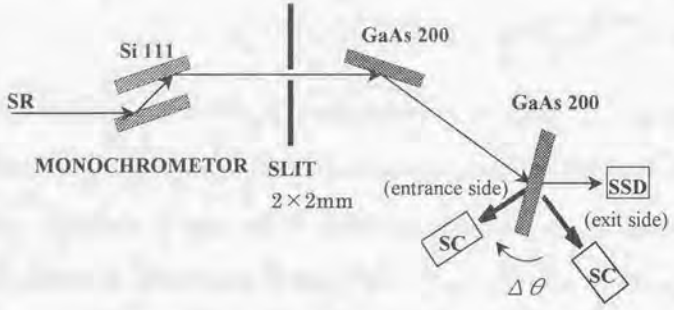

Fig 3.5 The schematic diagram of the experiment.

energy of 10502eV. The rocking curves of the fluorescence X-rays of (A), (B) and (C) were at the energy positions shown by the arrows of A, B, and C in Fig.3.2. The intensities of the rocking curves of (A), (B) and (C) decrease, when $\Delta\theta$ increases from negative, and show valley structure around $\Delta\theta$=0. In the curve (A), the intensity in the low angle side is higher than that in the high angle side. In the curve (B), intensities of the low angle side and the high angle side are almost equal. And in the curve (C), change of the intensity with respect to $\Delta\theta$ is reversed with the tendency of (A). Although the yield intensity of the fluorescence X-rays in the exit side was also measured, the intensity was too weak to see any systematic change[see curve (D)].

b) *Theory*

In symmetric Laue case, by assuming that the inelastic scattering, i.e., Compton scattering and thermal diffuse scattering (TDS) are negligible, the intensity of the fluorescence X-rays from depth z is proportional to $\left[\partial(P_h / P_o)/\partial z + \partial(P_d / P_o)/\partial z\right]$ at the crystal surface (Annaka, 1967[5]). The intensity of the fluorescence X-rays from the entrance surface of the crystal thickness H is given by the following equation

$$I_f = \int_0^H \left[\frac{\partial(P_h / P_o)}{\partial z}\right] e^{-\mu_f' z} dz + \int_0^H \left[\frac{\partial(P_d / P_o)}{\partial z}\right] e^{-\mu_f' z} dz . \tag{3.4}$$

Where, $\mu_f' = \mu_f / \cos\theta_f$, μ_f is the liner absorption coefficient of fluorescence X-rays, and θ_f is the angle between the surface normal and the detecting direction. The intensity of the fluorescence X-rays from the exit surface of the crystal is obtained by replacing $\exp(-\mu_f' z)$ by $\exp\left[-(H-z)\mu_f'\right]$ in (3.4), and is obtained. The fluorescence X-rays intensity in Laue case is given by the following equation

$$\begin{aligned} I_f = {} & (1-2p\sin\delta)\cdot \\ & \Big[\Big\{F1\cdot e^{-MH}\left[2s\,\mathrm{Re}\sqrt{Q}\sin(2sH\,\mathrm{Re}\sqrt{Q}) - M\cos(2sH\,\mathrm{Re}\sqrt{Q})\right] \\ & + F2\cdot e^{-MH}\left[-2s\,\mathrm{Re}\sqrt{Q}\sin(2sH\,\mathrm{Re}\sqrt{Q}) - M\sin(2sH\,\mathrm{Re}\sqrt{Q})\right] \\ & + M\cdot F1 + 2s\,\mathrm{Re}\sqrt{Q}\cdot F2\Big\} / MS2 \\ & + F3(e^{AH}-1)/A - F4(e^{-BH}-1)/B\Big] / (4|\sqrt{Q}|^2) . \end{aligned} \tag{3.5}$$

The parameters in (3.5) are given as follows.

$$Q = W^2 + 1 - 2q + 2ip\cos\delta , \tag{3.6}$$

$$p = \sqrt{q(1-q)} , \tag{3.7}$$

$$A = 2s\,\mathrm{Im}\sqrt{Q} - M, \tag{3.8}$$

$$B = 2s\,\mathrm{Im}\sqrt{Q} + M, \tag{3.9}$$

$$M = \mu' - \mu_f', \tag{3.10}$$

$$MS2 = M^2 + (2s\,\mathrm{Re}\sqrt{Q})^2, \tag{3.11}$$

$$F1 = 2\left[\mu'(|\sqrt{Q}|^2 - W^2 - 1) - 4Ws\,\mathrm{Re}\sqrt{Q}\,\mathrm{Im}\sqrt{Q}\right], \tag{3.12}$$

$$F2 = 4\left[s\,\mathrm{Re}\sqrt{Q}(|\sqrt{Q}|^2 - W^2 - 1) + \mu' W\,\mathrm{Im}\sqrt{Q}\right], \tag{3.13}$$

$$F3 = (2s\,\mathrm{Im}\sqrt{Q} - \mu')\left[2W\,\mathrm{Re}\sqrt{Q} - |\sqrt{Q}|^2 - W^2 - 1\right], \tag{3.14}$$

$$F4 = (2s\,\mathrm{Im}\sqrt{Q} + \mu')\left[2W\,\mathrm{Re}\sqrt{Q} + |\sqrt{Q}|^2 + W^2 + 1\right]. \tag{3.15}$$

Fig.3.7 shows the calculated result of fluorescence X-ray yield curve for GaAs200. The temperature parameter was used the result of Saravanan[6]. The convolution was carried out with the angle resolution of the crystal analyzer.

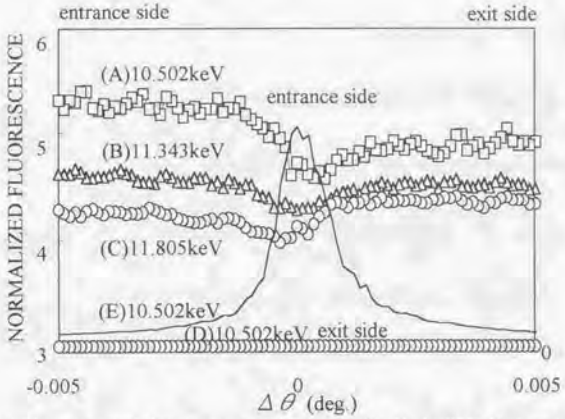

Fig 3.6 The measured fluorescence yield curves for GaAs 200. Curves (A), (B) and (C) represent the fluorescence yields near the entrance surface for $\chi_{hr}=-\chi_{hi}$, $\chi_{hr}=0$ and $-\chi_{hr}=-\chi_{hi}$, respectively; Curves (D) and (E) represent the fluorescence yield and the intensity of diffracted beam near the exit surface for $\chi_{hr}=-\chi_{hi}$.

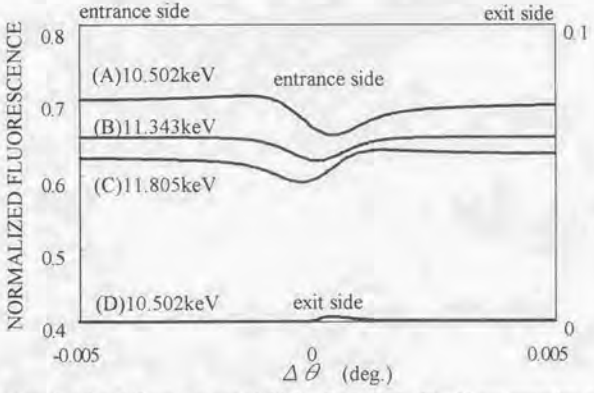

Fig 3.7 The simulated fluorescence yield for GaAs 200. The X-ray energies are (A)10.502KeV,(B) 11.343KeV and (C) 11.805KeV (D) 10.502KeV ,respectively.

c) *Discussion*

The calculated fluorescence X-rays yield curves in Fig.3.7 are in good agreement with the experimental result of Fig.3.6.

<In case of q= 1>

The linear absorption coefficient μ for $|W| \leq 1$ when $q= 1$ is shown in the following equation

$$\mu = \mu_0 \left(1 \pm \frac{|\chi_{hr}|}{\chi_{0i}} \sqrt{1 - W^2} \right). \tag{3.16}$$

Here, the plus sign is taken for the tie point 1, and minus sign for the tie point 2. Then for the tie point 1, $\mu > \mu_0$ and for the tie point 2, $\mu < \mu_0$.

X-rays corresponding to the tie point 2 show the anomalous transmission, and X-rays corresponding to the tie point 1 show the anomalous absorption. The calculated results of fluorescence X-ray yield in the entrance side are shown in Fig.3.8 for each tie point. The thin solid line shows the sum of the fluorescence X-ray yields for two tie points. The intensity curve of the fluorescence X-rays for the tie point 2 has a deep valley at $W= 0$, while the intensity curve of the fluorescence X-rays for the tie point 1 is flat. The valley structure in the yield(I_f) near $W= 0$ is attributed to the influence of the anomalous transmission from the experimental (Fig.3.6) and the calculation(Fig.3.7).

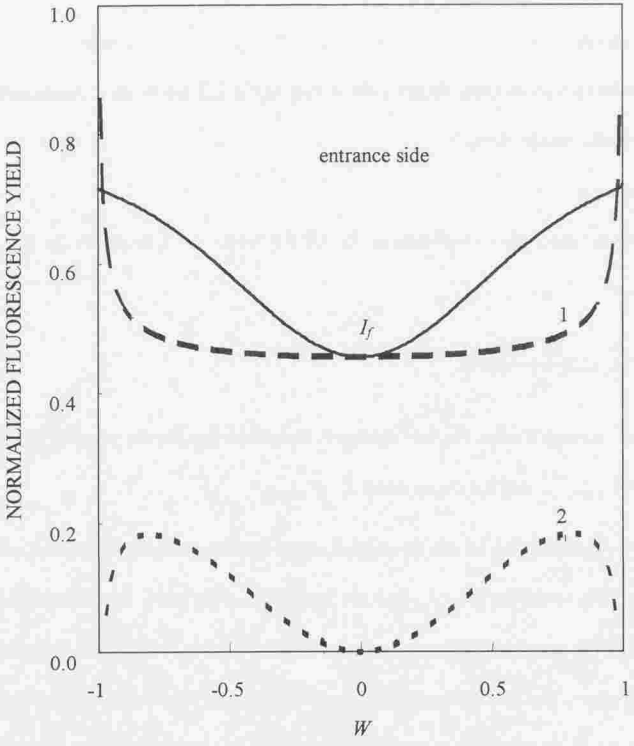

Fig 3.8 The fluorescence yield curves when q=1.

<In case of q= 0.5>

Similarly, in case of q= 0.5, the X-rays for the tie point 2 show the anomalous transmission, and X-rays for the tie point 1 show the anomalous absorption. The valley structures in the curves A and C in Fig.3.6 and the curves A and C in Fig.3.7 are due to anomalous transmission. As shown in Fig.2.6, the asymmetry in the rocking curve of the transmitted beam was reversed when δ changes from 0 to π. The reversal of the asymmetry in the fluorescence yield curves A and C in Fig.3.6 is due to the change of δ from 0 to π.

The study of the fluorescence X-ray yield curve in Laue case was carried out by Annaka (1967). He measured the fluorescence X-ray intensity from a perfect crystal of germanium using Mo K_α line. The valley structure due to anomalous transmission was observed and the reversal of the intensity difference between the low angle and the high angle side in Bragg angle was observed. Although the experimental result was to be analyzed by SIA theory, the relationship with δ was not investigated.

To our experimental results of fluorescence X-ray yield, SIA theory is not applicable. The experimental result only agrees well with calculation of this theory. Moreover, the change of the phase difference δ was also observed.

Conventionally, as for the determination of the atomic position of impurities, fluorescence X-rays in Bragg case under the condition that SIA theory is valid, have been used[7] [8] [9][10]. From the above mentioned result, it is concluded that the determination of the atomic position of impurities is possible also by observation of the fluorescence X-rays in Laue case.

3.4.2 Observation of δ and Dynamical Diffraction for $q < 0.5$

(i) Measured rocking curves of transmitted wave for GaAs 200

Since the energy of the region(1) in Fig.3.2 is lower than that of Ga and As *K*-absorption edges, the absorption coefficient is smaller than those in other regions. The q value is very small compared with 1. In such a region, it is difficult to observe the effect of anomalous transmission, but it is possible to observe of δ. An example of the calculated rocking curves are shown in Fig.3.9. q value is 0.05 in this case. The thick solid line and the thick dashed line are the rocking curves of the transmitted beam in case of $\delta = 0$ and $\delta = \pi$, respectively. The thin solid line is the rocking curve of the diffracted beam. The influence of δ is not

visible in the rocking curve of this diffracted beam. In case of $\delta = 0$ (thick solid line), the rocking curve of the transmitted beam serves as a valley in the central region at W=0, and the anomalous transmission is not seen. However, the intensity of the tail region of the rocking curve for $W < 0$ is higher than that of the region for $W > 0$. And in case of $\delta = \pi$, the intensity of the tail region for W<0 is lower than that for W>0 being opposite to the case of $\delta = 0$.

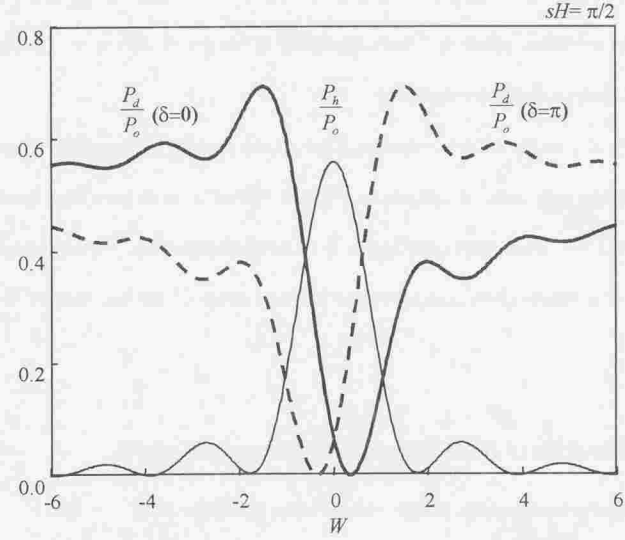

Fig.3.9 The calculated rocking curves in the symmetric Laue case for q=0.05, g_0=-1 and $sH = \pi/2$. The thin solid line is the curve of the diffracted beam. The thick solid and dashed lines are the curves of the transmitted beam for $\delta = 0$ and $\delta = \pi$, respectively.

The calculated value of χ_{hr} and χ_{hi} near the Ga K-absorption edge of GaAs are shown in Fig3.10. The solid lines represent the values of f'' determined from measurement of XANES and f' calculated using the dispersion relation in chapter I. The dashed lines represent those values obtained by the method of Parratt and Hempstead with the oscillator

strength of Cromer[11] (PHC). The dotted lines represent the calculated value by Sasaki[12] using the program of Cromer and Liberman[13](CLS). The energy points where χ_{hi} becomes zero differs in these three methods. The solid line becomes zero about −8.0eV from the edge, the dashed line at −3.7eV and the dotted line at 0eV. The measured rocking curves are shown in Fig3.11. The open circles(a) correspond to the energy at −5eV from the edge

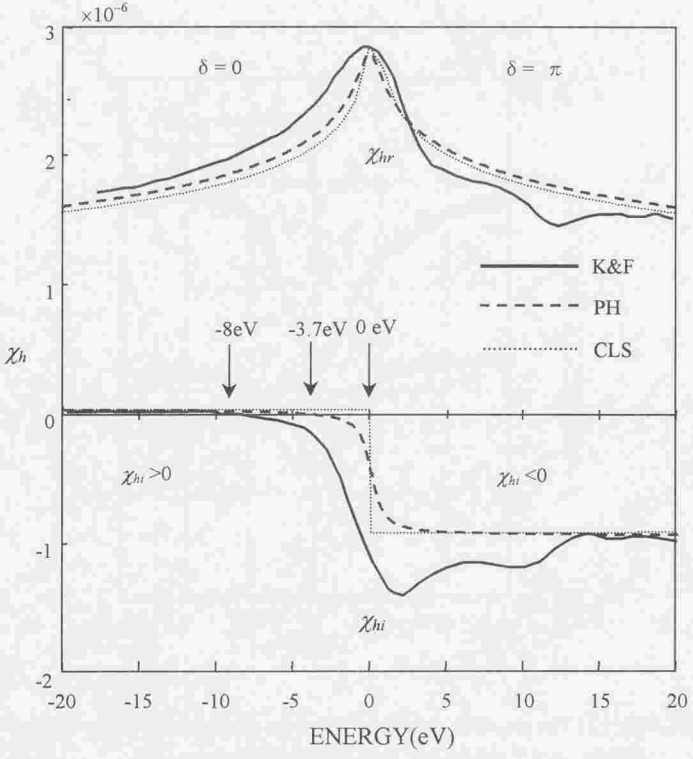

Fig.3.10 The Fourier coefficients of X-ray polarizability for GaAs 200. The solid lines, the dashed lines and the dotted lines show the curves obtained by the method of K&F, PH and CLS, respectively.

and the open triangles(b) –9eV. In (a), the intensity in the high angle side is larger than that in the low angle side, while in (b) the intensity in the low angle side is larger than that the high angle side. This clearly shows that δ changes from 0 to π, when the energy of X-rays changes from –9eV to –5eV below Ga *K*-absorption edge. And, in this energy range, there is the dynamical diffraction only due to χ_{hr} and χ_{hi}=0.

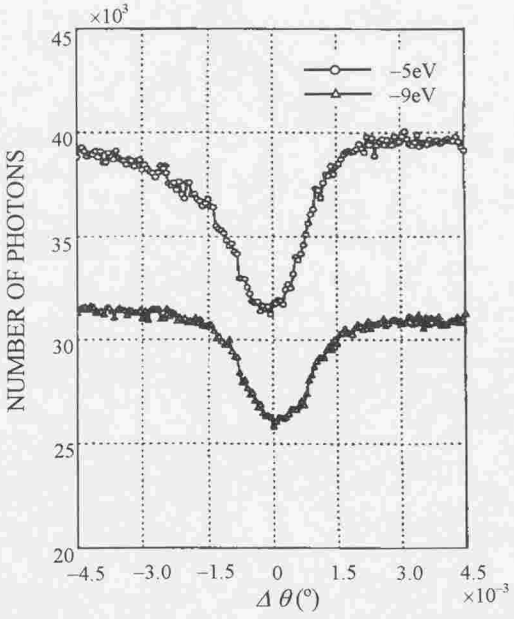

Fig 3.11 The measured rocking curves of the transmitted beam for GaAs. 200 for (a)-5eV and (b)-9eV from the Ga *K*-absorption edge.

(ii) **The measured and the simulated rocking curves for GaAs 600**

Observation of the phase change in the diffracted intensity in Bragg case has been

reported by Negishi *et al.*(1996) [14]. We describe it briefly in the following.

χ_{hr} and χ_{hi} near the Ga K-absorption edge of GaAs 600 are shown in Fig.3.12. The meanings of solid lines, dashed lines, and dotted lines are the same as that in Fig.3.10. The energies at which χ_{hi} becomes zero are −6.3eV(solid line), −3.5eV(dashed line) and 0eV(dotted line) from Ga *K*-absorption edge, respectively. In the Laue case, the energy position set to $\chi_{hi} = 0$ is in agreement with the experiment and the result with dispersion relation. Then, in the calculation of rocking curves in Bragg case, we use the anomalous scattering factor with the dispersion relation. The calculated rocking curves of the diffracted and transmitted beams are shown in Fig.3.13(a) and (b). (a) is the diffracted beams and (b) is the transmitted beams. In (a) and (b), the top curves are -9.0eV from the Ga *K*-absorption egde, the center curves are -6.3eV and the bottom curves are -3.0eV. The value of δ is 0 at −9eV from Ga *K*-absorption edge, and is π at −3eV. The diffracted rocking curve shows the peak almost in the center, and the transmitted rocking curve shows the valley. The rocking curves of the diffracted beam and the transmitted beam are asymmetric except for the energy point of $\chi_{hi}=0$ (−6eV). For the energy of $\chi_{hi}>0$(−9eV), the peak of the diffracted beam slightly shifts to the low angle side from the exact Bragg angle. The intensity of the tail of the transmitted beam in the low angle side is higher than that in the high angle side. For the energy of $\chi_{hi}<0$ (−3eV), the asymmetry of the rocking curve reverses both in the diffracted beam and the transmitted beam. The reason why this asymmetry reverses is that δ in (2.62) change from 0 to π. That is, $\delta = 0$ because of $\chi_{hi}>0$, and $\delta = \pi$ because of $\chi_{hi}<0$.

The experiment was carried out by using X-rays from SR in KEK-PF, BL-6C1. SR monochromated by Si 333 double-crystal monochromator is incident on the sample crystal of GaAs. The intensities of 600 diffracted and transmitted beams in the Bragg case are similutaneously measured with SC and SSD, respectively.

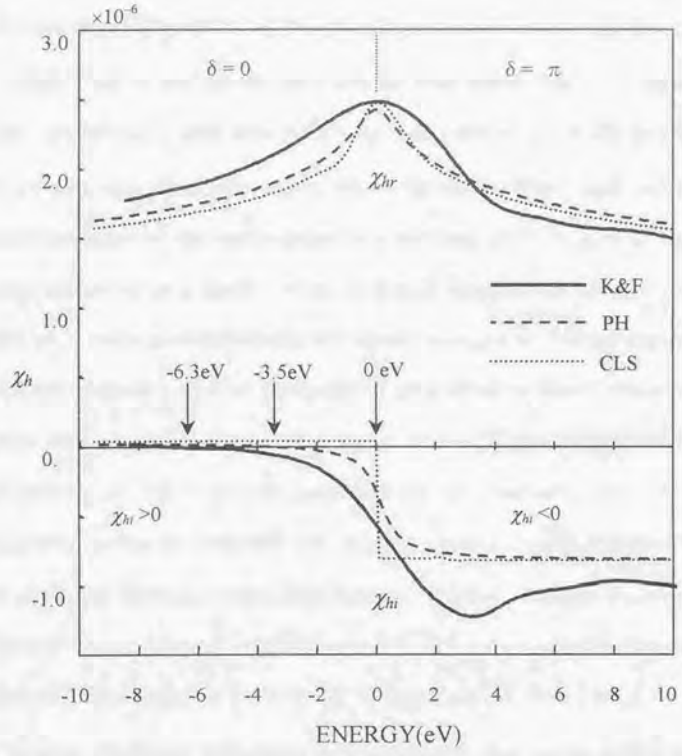

Fig.3.12 The Fourier coefficients of X-ray polarizability for GaAs 600. The solid lines, the dashed lines and the dotted lines show the curves obtained by the method of K&F, PH and CLS, respectively.

The measured rocking curves are shown in Fig.3.14. The energies of the incident X-ray is (a)–9eV, (b)–6eV and (c)–3eV from Ge *K*-absorption edge. The half width of the measured diffracted rocking curve is about 6×10^{-4} deg. The half width of the calculated diffracted

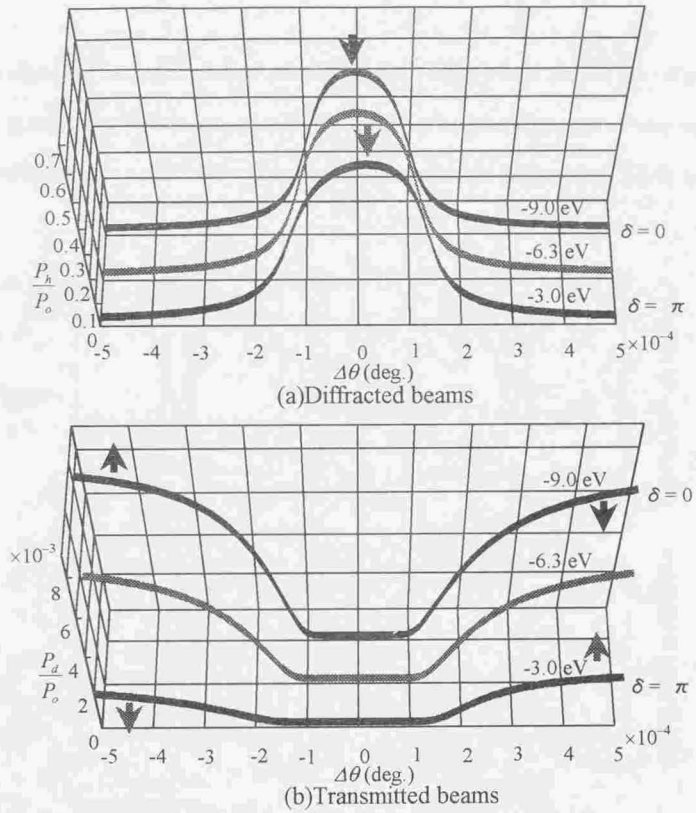

Fig.3.13 The calculated rocking curves of the diffracted(a) and the transmitted (b) beams in the symmetric Bragg case for GaAs 600 of thickness 134μm. The arrows in (a) indicate the peak positions. The upward arrows in (b) indicate the higher intensities than the average and the downward arrows the lower intensities.

rocking curve is about 6×10^{-5}deg.(Fig3.13). This calculated half width is smaller by about 1/10 than the measured value. Under the experimental condition, the tendency of the peak shift of the diffracted beam cannot be distinguished clearly in the rocking curves of (a) - (c).

As for the rocking curves of the transmitted beam, the intensity in the low angle side is larger than the high angle side in Fig.3.14(a). However the asymmetric tendency is reversed in (c). In (b), the intensities in the low angle side and high angle side are almost the same.

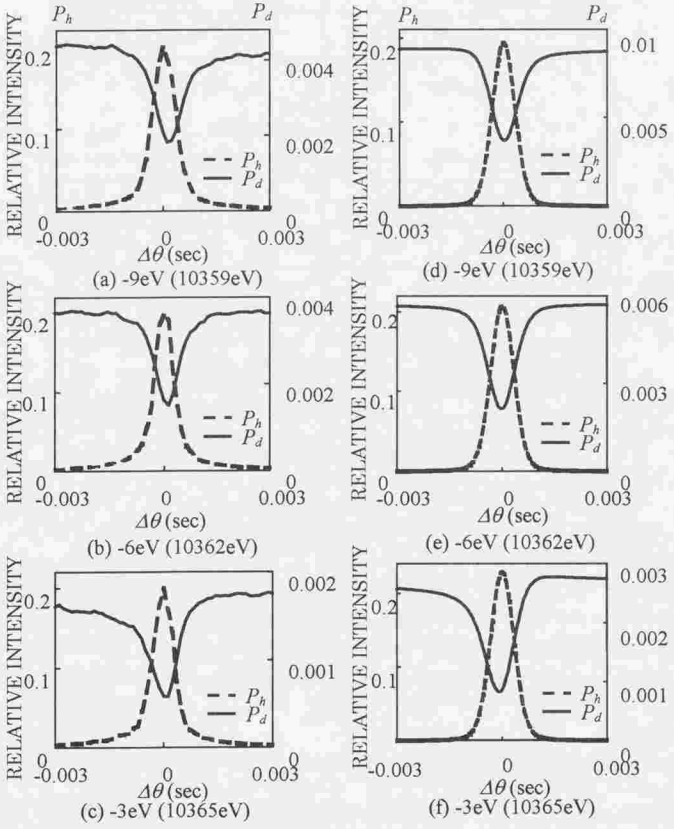

Fig.3.14 The measured and the simulated rocking curves for GaAs 600. The dashed and the solid curves corresponding to the diffracted(left scale) and the transmitted (right scale) beams, respectively. (a),(b) and (c) are experimental results. (d),(e) and (f) are the convoluted curves by using anomalous scattering factor of KF.

The corresponding results of conclution of the rocking curve are shown in Fig.3.14 (d),(e) and (f). The asymmetry in (a) and (c) is the same as that in (d) and (f), respectively. Therefore, it is concluded that $\delta = 0$ in (a), $\delta = \pi$ in (c) and $\chi_{hi} \approx 0$ in (b).

According to the above two considerations[Laue case(i) and Bragg case(ii)] both from theory and the experiment on the transmitted rocking curve in the energy below the Ga *K*-absorption edge, the agreement between theory and an experiment is quite. Thus, the theory of this paper also is valid in case of $q<0.5$.

3.5 **Improvement of Dislocation Contrast in Topography**

3.5.1 Introductory

The topographs from GaAs single crystals were observed by using X-rays from SR in two extreme cases. In one case, by tuning the X-ray energy near *K*-absorption edge of Ga and As, χ_{hr} was set to be zero and only χ_{hi} contributed to contrast($q\approx1$) to enhance the Borrmann effect[15]. In the other case, χ_{hr} mostly contributed the contrast($q\approx0$).

3.5.2 Experiment

The experimental arrangement is shown in Fig.3.15. The diffracted beam was monitored by SC and the transmitted beam was monitored by SSD, respectively. The photograph of the penetration X-ray image was taken using a nuclear plate.

Fig3.16 is the topographies taken for $q \approx 1$(a), and $q \approx 0$(b). The pattern of the photograph come from dislocations. The white part in the photograph (a) is a part where the X-ray intensity is strong according to Borrmann effect, and two black spots are visible clearly. However, in (b), the contrast of the photograph is weak. As for the dislocation image of the transmitted beam in case of $q \approx 1$, the contrast was enhanced according to Borrmann effect in comparison with the image of $q \approx 0$.

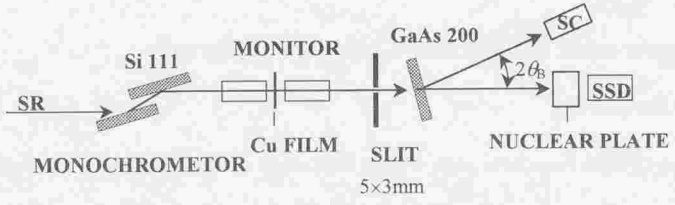

Fig 3.15 Schematic diagram of the measuring system for the topograph.

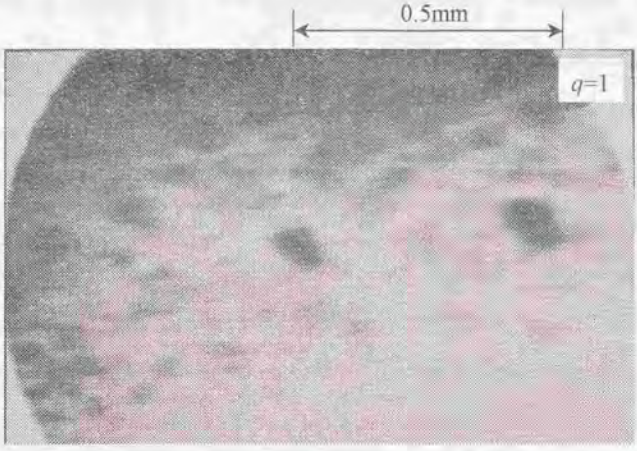

(a)

(b)

Fig 3.16 X-ray topographies of the transmitted beam when q=1(a) and q=0.0004(b)

3.6 Determination of Anomalous-Scattering Factors by Using Transmitted Rocking Curves near the Absorption Edge

3.6.1 Introductory

In order to determine atomic scattering factors of X-rays by measuring rocking curves, it is nessary to use very parallel beam of X-rays. Kohra and Kikuta[16] obtained extremely parallel beams by using multi-crystal monochromator under the condition of an asymmetric reflection for Cu characteristic X-rays. Then they investigated the slight difference between the calculated rocking curves and the observed ones and determined atomic scattering factors of Si by measuring the rocking curves of the diffracted beam in the Bragg case. On the other hand, Kawamura and Fukamachi[17] determined anomalous scattering factor $f''(\omega)$ by measuring the linear absorption coefficient and then $f'(\omega)$ by using the dispersion relation very near the absorption edge of Ni.

In the present section, the rocking curves of the diffracted and the transmitted beams of GaAs 200 have been measured at BL-6C1, KEK-PF in the symmetric Laue case around the Ga K-absorption edge. The changes of the transmitted rocking curves become conspicuous as compared with those of the diffracted curves very close to the edge. This indicates that the profile fitting method is applicable to determination of the anomalous scattering factors, and the anomalous scattering factors of Ga have been obtained by using the fitting method[18]. These results are compared with the values obtained by three methods. The first values were calculated by using PHC, the second values were calculated ones by CLS and the third values were those obtained by Fukamachi *et al.*(FHKO)[19]. In the third method, $f''(\omega)$ was obtained from the measured linear absorption coefficient and $f'(\omega)$ was calculated by using the dispersion relation.

3.6.2 Experiment

The experimental system and the experimental method are the same as that of Section 3.3. The transmitted rocking curves are shown in Fig. 3.17(a), which were measured at the indicated energies below the Ga K-absorption edge. In Fig. 3.17(c), those measured above the edge are shown. The data have been normalized by the integrated reflecting power of the diffracted beam. In Fig. 3.17(a), the transmitted rocking curve shows a valley for X-ray energy ω = 10357.2 eV, but a peak instead of the valley for ω = 10365.6 eV. As is well known, the peaks are due to anomalous transmission.

In the rocking curves of the transmitted beam when ω = 10357.2 eV, it is seen that the intensities in the low angle side are higher than those in the high angle side. In contrast, when ω > 10357.2 eV, the intensities in the high angle side are higher than those in the low angle side. The reversal of the asymmetry is due to the change of the phase of the crystal structure factor [2].

Here we can see clearly that the changes of the transmitted rocking curves below the Ga K-absorption edge due to the anomalous-scattering are very remarkable. On the other hand, above the edge, the central peak gradually increases with increasing the X-ray energy as shown in Fig. 3.17(c). The intensities of the tail in the high angle side are higher than those in the low angle side. But we are not able to see the obvious changes like in Fig.3.17(a).

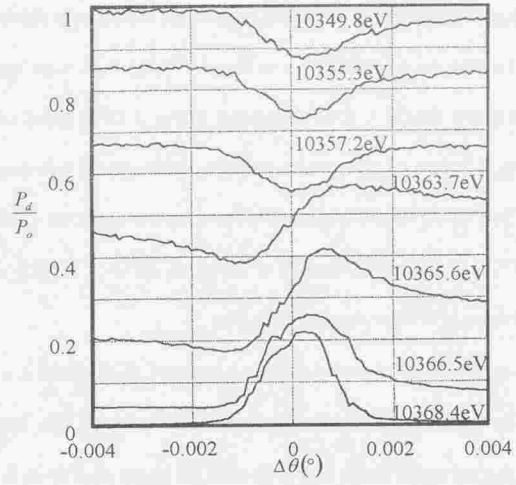
10349.8eV
10355.3eV
10357.2eV
10363.7eV
10365.6eV
10366.5eV
10368.4eV
1
0.8
0.6
0.4
0.2
0
$\frac{P_d}{P_o}$
-0.004
-0.002
0
0.002
0.004
$\Delta\theta(°)$

(a)

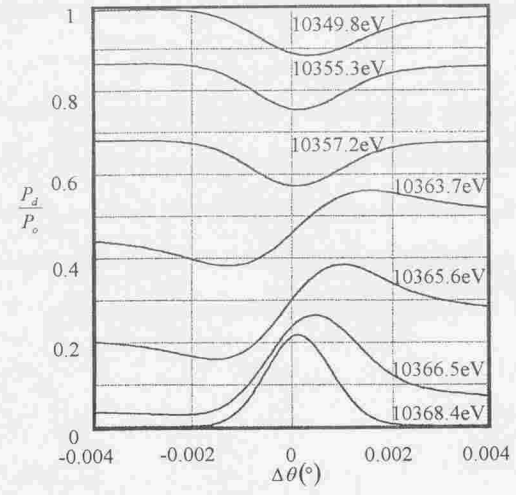
10349.8eV
10355.3eV
10357.2eV
10363.7eV
10365.6eV
10366.5eV
10368.4eV
1
0.8
0.6
0.4
0.2
0
$\frac{P_d}{P_o}$
-0.004
-0.002
0
0.002
0.004
$\Delta\theta(°)$

(b)

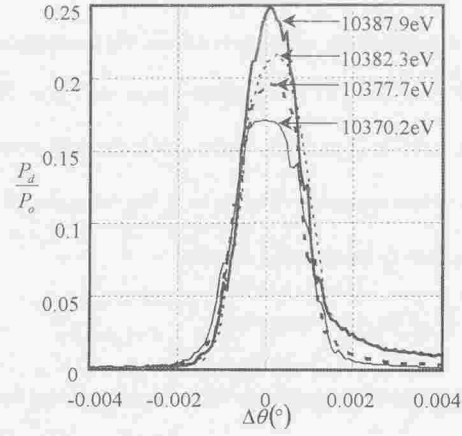

(c)

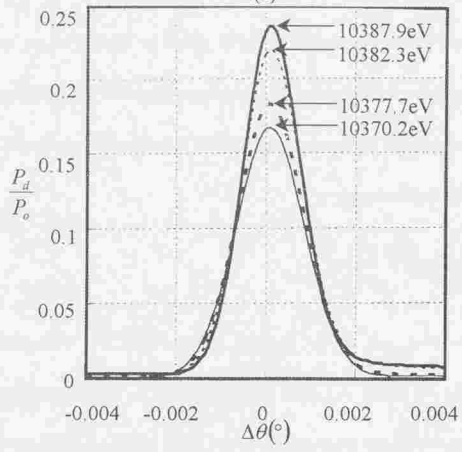

(d)

Fig.3.17 The rocking curves of the transmitted beam for GaAs 200. (a) The measured rccking curves and (b) the fitted ones below the Ga K-absorption edge, (c) the measured rocking curves and (d) the fitted ones above the edge.

3.6.3 Fitting Analysis

The procedure in the profile fitting method is as follows. We denote the normalized intensity of the measured rocking curve of the transmitted beam as $I_{obs}(\omega, \Delta\theta)$ and that of the calculated rocking curve as $I_{cal}(\omega, \Delta\theta)$. Here, $\Delta\theta$ is the shift from the Bragg angle. $I_{cal}(\omega, \Delta\theta)$ can be written approximately in the form: The rocking curve $I_{cal}(\omega, \Delta\theta)$ of the transmitted beam is given by the following equation

$$I_{cal}(\omega, \Delta\theta) = \int_{-\infty}^{+\infty} \frac{P_d}{P_o}(\omega, \Delta\theta - x) g(x, \sigma) dx . \qquad (3.17)$$

Here, $P_d/P_0(\omega, \Delta\theta)$ is calculated using the dynamical theory assuming that the incident beam is an ideal plane wave. P_d is the intensity of the transmitted beam and P_0 that of the incident beam. The intensity of dynamical diffraction is given by (2.82b). $g(x, \sigma)$ is a convolution function which is used in order to take the dispersive angle of the incident wave into account so that the calculated results can be compared with the experimental ones. To approximation, we adopt a Gaussian function, *i.e.*

$$g(x, \sigma) = \frac{1}{\sigma\sqrt{\pi}} \exp\left(-\frac{x^2}{\sigma^2}\right). \qquad (3.18)$$

Therefore we can write $I_{cal}(\omega, \Delta\theta) = I_{cal}(\Delta\theta, f'(\omega), f''(\omega), \sigma)$. The profile fitting has been carried out in order to bring I_{cal} into accord with I_{obs}, the normalized intensity of the measured rocking curve of the transmitted beam, by a trial and error method with which we repeatedly adjusted the values of $f'(\omega), f''(\omega)$ and σ until the deviation can be evaluated as its minimum value.

The fitted results are shown in Fig. 3.17(b) and (d). In this way, we obtained the values of $f_{Ga}'(\omega)$ and $f_{Ga}''(\omega)$ within 1% of the error which are shown in Fig. 3.18, and $\sigma = 0.0011° \pm 0.0003°$.

3.6.4 Results and discussion

By making a comparison between the measured rocking curves and the fitted ones (refer to Fig.3.17), it is clear that the measured result is generally in good agreement with the fitted result, but the agreement above the Ga K-absorption edge is not as good as that below the edge.

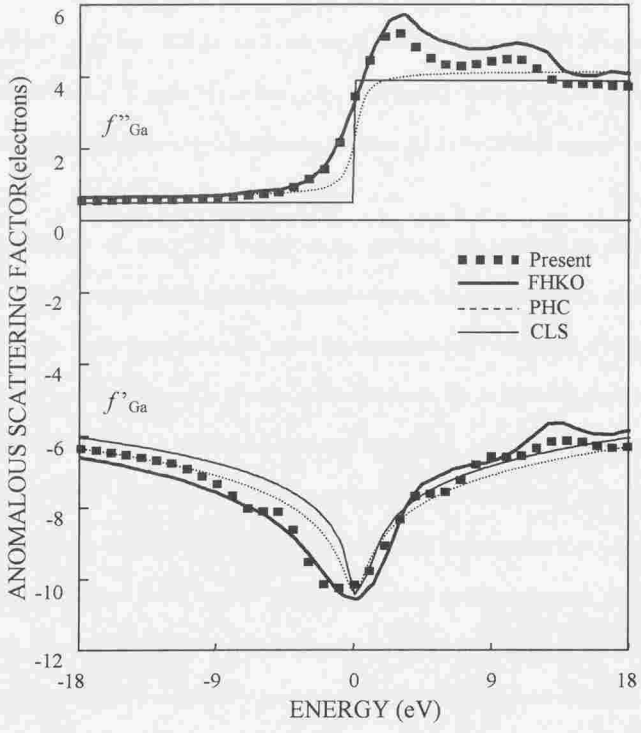

Fig.3.18 The values of f' and f'' of Ga near the Ga K-absorption edge. The squares are the present result, the thick solid lines are the FHKO result, the thin dashed lines are the PHC result and the thin solid lines are the CLS result. The abscissa is the energy from the Ga K-absorption edge.

Fig. 3.18 shows the values of $f'(\omega)$ and $f''(\omega)$ obtained from the fitting together with those of FHKO, PHC and CLS. The results of curve fitting are in agreement with the results of FHKO. Furthermore, above the edge, two peaks in the curve of $f''(\omega)$ are seen both in the results of FHKO and the present fitting, which can be explained as XANES. In the energy region from the edge to –10 eV, the $f'(\omega)$ values of FHKO are slightly less than those of PHC or CLS. A similar tendency is seen in the present result. Above the edge, the $f'(\omega)$ values of FHKO are more or less larger than those of PHC and CLS. This tendency is the same as the present one. Accordingly, very close to the edge, the calculated anomalous scattering factors by PHC and CLS methods are not suitable to explain the phenomena for a real crystal.

In order to improve the accuracy of anomalous scattering factors, we have two possibilities. One is to use the incident beam of smaller dispersive angle. In the present experiment, if the incident monochromatized beam is an ideal plane wave, the full width at half maximum (FWHM) of the calculated rocking curves of the diffracted beam of GaAs 200 is about 1 second (see Fig. 3.19). But the observed FWHM is about 6 seconds, 6 times larger than that of the ideal case. The main reason why this FWHM broadens is the intrinsic width of the monochromatized beam. Kohra and Kikuta[16] had held down the dispersive angle of the monochromatized beams to about 0.1 seconds which were much smaller than that of the diffracted beam from the sample. Thus, they were able to deal with the rocking curves without convolution and investigated the slight difference between the results of the calculation and the measurement. In the present experiment, we cannot deal with the rocking curves as Kohra and Kikuta[16] did, because the dispersive angle of the monochromatized beam is much larger than that from the sample. But we can use the rocking curves of the transmitted beam instead of those of the diffracted beam, because the change of the

transmitted rocking curves is conspicuous as compared with that of the diffracted ones. The other possibility is to use a thinner sample crystal, which enhances the change of the transmitted curves above the absorption edge.

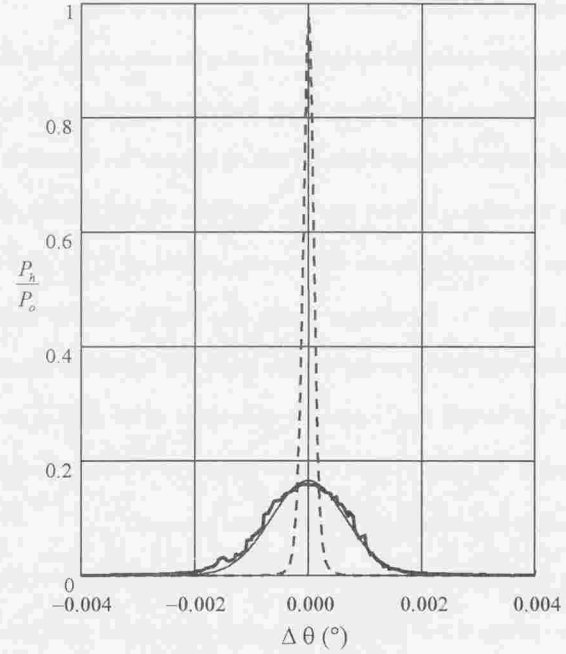

Fig.3.19 The rocking curves for the diffracted beam of GaAs 200 at 10387.6eV. The thick solid line is measured one, the dashed line is the calculated one for an ideal plane wave and the thin solid line is the calculated one with convolution.

3.7 Summary

In 3.1, integrated reflecting powers are measured for Ge 844. f^0 from the measurement, it is found that and $|f'|$ become equal and $f^0 + f' = 0$ at −2.8eV below Ge *K*-absorption

edge. The dynamical diffraction only due to $f''(\omega)$ predicted theoretically is measured.

In 3.2, χ_{hr} and χ_{hi} for GaAs 200 was discuss near Ga and As K-absorption edge. The changes of the signs of χ_{hr} and χ_{hi} and the phase δ are studied theoretically as a function of X-ray energy. The result shows that the measurement of be useful to confirm dynamical diffraction GaAs 200 reflection should predicted by this theory.

In 3.3, the experiment system and the specimen used in the measurement are described.

In 3.4, the measurements of the rocking curves, fluorescence yields and the topographies from GaAs were studied. From observation of rocking curves of the transmitted beam, the value of δ was determine to be either 0 or π in case of q= 0.5, and the X-ray energy was determined where dynamical diffraction only due to χ_{hi} (that is, q= 1) was generated. Next the theoretical formula for fluorescence X-rays was derived, and the corresponding experiment is performed. The agreement between theory and experiment was quite good. Furthermore, it was verified from continuous observation of the rocking curve of the transmitted beam in the range $0<q\leq 0.5$ that δ takes 0 or π. And it verified that the dynamical diffraction only due to χ_{hr} (that is, q= 0) was generated.

In 3.5, using GaAs, the topograph of the transmitted beam in in case of $q \approx 0$ in the slightly lower energy region from Ga K-absorption edge was observed, and it was compared with the topograph of the transmitted beam in case of $q \approx 1$ at the energy between Ga K-absorption and As K-absorption edges. It is shown that the contrast of the dislocation image enhanced in the topograph for $q \approx 1$ as compared with that for $q \approx 0$.

In 3.6, the rocking curve was measured by 1eV step across Ga K-absorption edge. A profile fitting method was applied determination of $f'_{Ge}(\omega)$ and $f''_{Ge}(\omega)$ from the rocking curve of the transmitted beam. Two clear peaks were observed in the curve of

$f''_{Ge}(\omega)$. These peaks correspond to XANES. $f'_{Ge}(\omega)$ should good agreement with the calculated result. Then rocking curves were measured using the incident beam with the dispersion angle also of 6 times larger than the half width of the diffracted beam from the sample. Nevertheless, the measured results of anomalous scattering factors comparatively high accuracy were obtained. If the dispersion angle of the incident beam is made smaller than the half width of the diffracted wave from the specimen, the accuracy in the measurement of the anomalous-scattering factor will be improved remarkably.

As mentioned above, it was shown in experiments of chapter III that the dynamical diffraction only due to χ_{hi} is observed not only in a monatomic crystal, but also a biatomic crystal. It was also shown that in a biatomic crystal the dynamical diffraction only due to χ_{hr} is observed. The validity of the present theory was shown in the case when the changes in χ_{hr} and χ_{hi} were large. As for the rocking curve of the dynamical diffraction only due to χ_{hi} in Bragg case, the half width of the rocking curve is quite small compared with that only due to χ_{hr}. Therefore, in order to investigate in detail the result considered in this paper, the resolution of the experimental equipment of the conventional dynamical diffraction is not enough. In order to carry out the study of the dynamical diffraction only due to χ_{hi} considered in this paper in detail, the improvement in the resolution of an optical system must be achieved.

APPENDIX C: **Fluorescence X-rays**

In order to calculate and translate, P_h / P_o and P_d / P_o are modified as follows on symmetrical reflective conditions

$$\frac{P_h}{P_o} = \frac{1-2p\sin\delta}{4|\sqrt{Q}|^2}\left[e^{(2s\,\mathrm{Im}\sqrt{Q}-\mu')z} + e^{-(2s\,\mathrm{Im}\sqrt{Q}+\mu')z} - 2e^{-\mu' z}\cos(2sz\,\mathrm{Re}\sqrt{Q})\right], \qquad \text{(c1)}$$

$$\begin{aligned}\frac{P_d}{P_o} = \frac{1}{4|\sqrt{Q}|^2}\Big\{&(|\sqrt{Q}|^2+W^2)\left[e^{(2s\,\mathrm{Im}\sqrt{Q}-\mu')z} + e^{-(2s\,\mathrm{Im}\sqrt{Q}+\mu')z}\right]\\ &-2W\,\mathrm{Re}\sqrt{Q}\left[e^{(2s\,\mathrm{Im}\sqrt{Q}-\mu')z} - e^{-(2s\,\mathrm{Im}\sqrt{Q}+\mu')z}\right]\\ &+4W\,\mathrm{Im}\sqrt{Q}e^{-\mu' z}\sin(2sz\,\mathrm{Re}\sqrt{Q})\\ &+2(|\sqrt{Q}|^2-W^2)e^{-\mu' z}\cos(2sz\,\mathrm{Re}\sqrt{Q})\Big\}.\end{aligned} \qquad \text{(c2)}$$

(c1) and (c2) are calculated using $\frac{\partial(P_h / P_o)}{\partial z}$ and $\frac{\partial(P_d / P_o)}{\partial z}$, and the fluorescence X-ray yield intensity I_f is calculated using (3.4).

References

[1] T. Fukamachi, R. Negishi, M. Yoshizawa, K. Ehara, T. Kawamura, T. Nakajima and Z. Zhao(1993)"*X-ray Dynamical Diffraction in Ge with a Zero-Real-Part Scattering Factor*", *Acta Cryst.*, A**59**, 573-575.

[2] T. Fukamachi, R. Negishi, S. Zhou, M. Yoshizawa, T. Sakamaki, T. Kawamura and T. Nakajima(1996)"*Observation of Change of X-ray Polarizability in Rocking Curves*", *Acta Cryst.*, A**52**, 669-674.

[3] M. Yoshizawa, T. Fukamachi, K. Ehara, T. Kawamura and K. Hayakawa(1988) "*Observation of Pendellösung Fringes Induced by X-ray Resonant Scattering*", *Acta Cryst.*, A**44**, 433-436.

[4] R. Negishi, T. Fukamachi, Z. Xu, M. Yoshizawa, I. Matsumoto, T. Kawamura and T. Nakajima(1996)"*X-ray Fluorescence Yield with Strong Borrmann Absorption in the Laue Case*", *KEK Progress Report 96-3 A/M* ,111.

[5] S. Annaka(1967)"*Intensity Anomaly of Fluorescent X-Ray Emission Accompanying the Laue Case Reflection from a Perfect Crystal*", *J. Phys. Soc. Japan*, **23**, 372-377.

[6] R. Saravanan,S. K. Mohanlal and K. S. Chandrasekaran(1992)"*Anharmonic Temperature Factors, Anomalous-Dispersion Effects and Bonding Charges in Gallium Arsenide*", *Acta Cryst.*,A**48**,4-9.

[7] B. W. Battermann(1969)"*Detection of Foreign Atom Sites by their X-Rays Fluorescence Scattering*", *Phys. Rev. Lett.*, **22**, 703-705.

[8] J. A. Golovchenko, B. W. Battermann and W. L. Brown(1974)"*Obsevation of Internal X-Ray Wave Fields During Bragg Diffraction with an Application to Impurity Lattice Location*", *Phys. Rev.*, **B10**, 4239-4243

[9] S. K. Andersen, J. A. Golovchenko and G. Mair(1976)"*New Application of X-Ray Standing-Wave Fields to Solid State Physics*", *Phys. Rev. Lett.*, **37**, 1141-1145.

[10] K. Akimoto, T. Ishikawa, T. Takahashi and S. Kikuta(1985)"*Structural Analysis of the $NiSi_2$/(111)Si Interface by the X-ray Standing-Wave Method*",*Jpn. J. Appl. Phys.*, **24**, 1425-1431.

[11] L. G. Parratt and C. F. Hempstead(1954)"*Anomalous Dispersion and Scattering of X-Rays*", *Phys.Rev.*,**94**,1593-1600.

D. T. Cromer(1965)"*Anomalous Dispersion Corrections Computed from Self-Consistent Field Relativistic Dirac-Slater Wave Functions*", *Acta.Cryst.*,**18**,17-23.

[12] S. Sasaki(1989)"*Numerical Tables Anomalous Scattering Factors Calculated by the Cromer and Libermans Method*", *KEK Report 88-14 M/D*, 1-136.

[13] D. T. Cromer and D. Liberman(1970)"*Relativistic Calculation of Anomalous Scattering Factors for X-Rays*", *J. Chem. Phys.* **53**, 1891-1898.

[14] R.Negishi, T.Fukamachi, S.M.Zhou, Z.C.Xu, M.Yoshizawa, I.Matsumoto, T.Sakamaki, T.Kawamura and T.Nakajima(1997)"*Observation of Phase Change of X-ray Polarizability by the Rocking Curves in the Bragg case*", *Acta Cryst.*

[15] R. Negishi, T. Fukamachi, T. Kawamura, M. Yoshizawa, T. Nakajima and K. Ehara (1994)"*Improvement of Dislocation Contrast be Use of Borrmann Effect*", *KEK Progress Report* **94-1** A/M,145.

[16] K. Kohra and S. Kikuta(1968), Acta Cryst. **A24**, 200-.

[17] T. Kawamura and T. Fukamachi(1978), *Proc. Int. Conf. X-Ray and XUV Spectroscopy, Sendai*, 1978, *Jpn. J. Appl. Phys.* **17**, 224.

[18] S. Zhou, M. Yoshizawa, T. Fukamachi, R. Negishi, K. Ehara, T. Kawamura and T. Nakajima(1997)"*Determination of the Anomalous Scattering Factors by Using Transmitted Rocking Curves near the Absorpyion Edge*", *Jpn. J. Appl. Phys.*(in press).

[19] T. Fukamachi, S.Hosoya, T.Kawamura and M.Okunuki(1977)"*X-Ray Intensity Measurements on Large Crystals by Energy-Dispersive Diffractometry. III. Fine Structures of Integrated Intensities and Anomalous Scattering Factors near the K Absorption Edges in GaAs*", *Acta Cryst.*, A**33**,54-58.

CHAPTER IV CONCLUSION AND FUTURE VIEW

4.1 Conclusion

In the treatment of the conventional dynamical diffraction, the ordinal scattering was subjective and the X-ray resonance scattering was auxiliary. However, SR appears now and the dynamical diffraction which united the energy of the incident X-ray with the energy of *K*-absorption edge of a atom which constitutes a crystal come to be obtained. For this reason, in the dynamical diffraction, there is a case in which a X-ray resonance scattering becomes subjective from a normal scattering. In this paper, I considered and analyzed from sides of the theory and the experiment including the case which a X-ray resonance scattering becomes subjective.

The conventional dynamical theory (SIA) to which approximation of $|\chi_{hr}|>|\chi_{hi}|$ is applied is not helpful at all in the study of the dynamical diffraction by the X-ray resonance scattering accompanied in the case of $\chi_{hr}=0$. For this reason, Fukamachi and Kawamura presented a theory to calculates the exact dynamical diffraction which does not carry out approximation like SIA. In this study, I extended the dynamical diffraction by the X-ray resonance scattering on the basis of the theory of Fukamachi and Kawamura, and derived the formula of the diffracted intensity for a finite thickness crystal in Laue case and Bragg case

I examined the phenomena which is anticipated by the fundamental equation: such us the complex dispersion surface, the poynting vector, and the wave field in a crystal. I obtained the results which cannot be expects at all by SIA, newly, the similarity between the dispersion surface of Bragg case of $q=0$ and Laue case of $q=1$, the fact that the poynting vector does not intersect perpendicularly to the dispersion surface, and the

useful result about Borrmann effect in the dynamical diffraction only due to χ_{hi}.

The experimental work of X-ray resonance scattering has been carried out in BL6C1 of KEK-PF in the dynamical diffraction by using the diffractometer of our own making with the Si(111) double-crystal monochromator. We succeeded in the observation of phase difference δ, and confirmed that the dynamical diffraction only due to χ_{hi} or χ_{hr}. It was shown that the theory developed in CHAPTER II is verified by the experiment using SR, and it is valuable to research of the dynamical diffraction accompanied by an X-ray resonance scattering as measurement of a anomalous-scattering factor.

4.2 Future View

According to theory described in CHAPTER II, SIA is applicable to the range of $|\chi_{hi}|/|\chi_{hr}| \leq 0.1$, or range of $q \leq 0.01$. It is clear that the range of q are 0~1. If the range of q sets 0~100%, the study of the dynamical diffraction by the conventional SIA corresponds to 0~1%. That is, the theory of this paper remains and is useful to 99% study of the field. Therefore, it is no wonder that new phenomena and new effects should be discovered by the future study from the wide study field left by SIA.

The theories and experiments presented in this paper will be useful to elucidate such the enigma at present as increase of the anomalous transmission in asymmetrical reflection[1] and the reflection reflecting polarity is excepted, and interesting study is expected also in the field.

Moreover, not only the application to the Thompson scattering and the resonance scattering of X-rays, the result of this paper is also applicable to a neutron scattering[2] when the imaginary part of the scattering length b is large, and the nuclear Bragg scattering[3] in the case $q = 1$.

References

[1] S. Kishino(1971)"*Anomalous Transmission in Bragg-case Diffraction of X-rays*", *J. Phys. Soc. Jpn.*, **31**, 1168-1173.

S. Kishino(1974)"Enhanced Sensitivity of Anomalously Transmitted Intensity to Lattice Defects in Asymmetric Bragg-case Diffraction of X-rays", *Jpn. J. Appl. Phys.*, **13**, 587-593.

[2] International Table for X-ray Crysrallography(1968), Vol.**IV**,228-231, Birmingham, KYNOCH PRESS.

[3] S. Kikuta(1995)"*Nuclear Resonant Scattering Using Synchrotron Radiation*", *Butsuri*, **50**, 630-636(in Japanese).

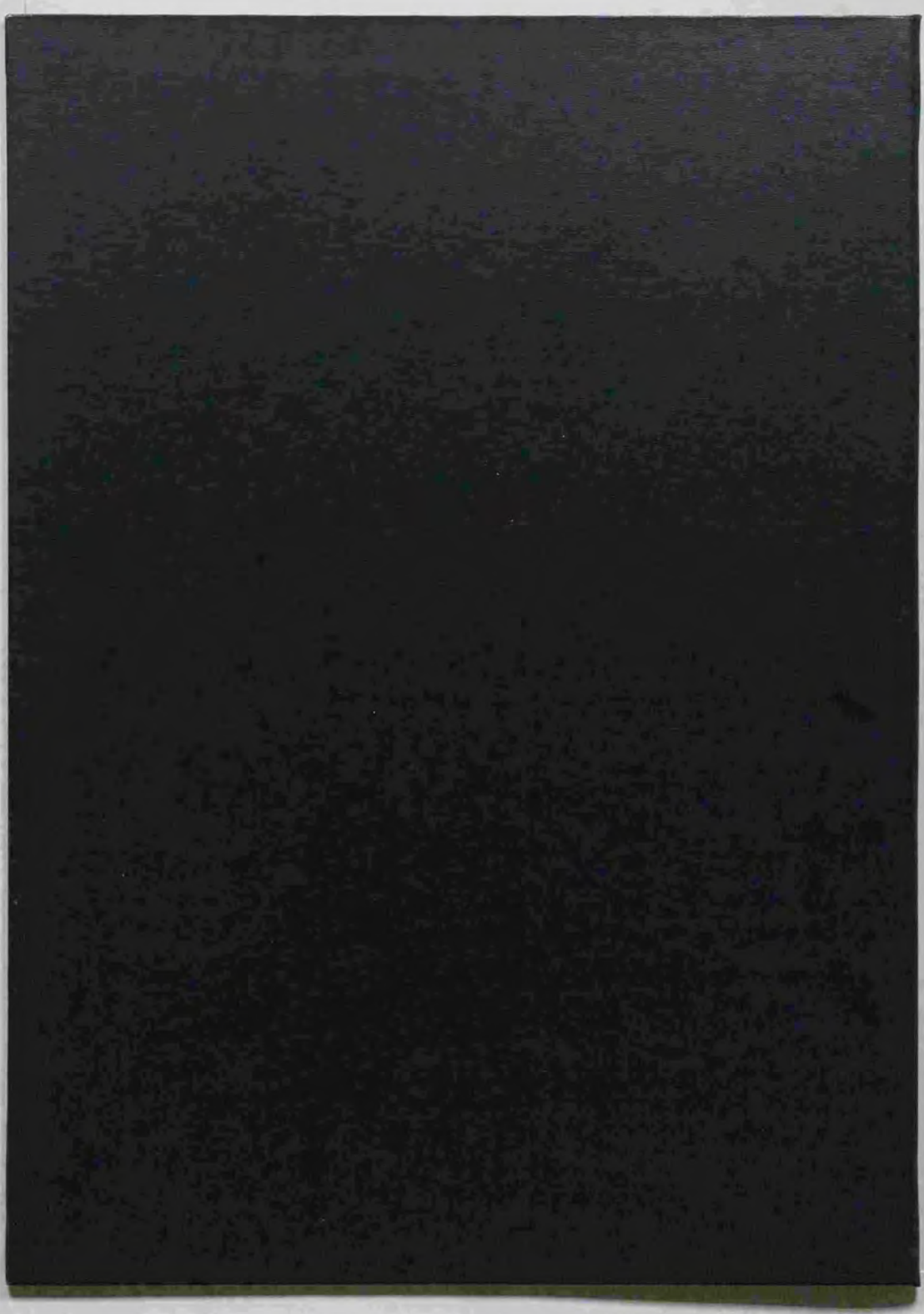

Kodak Color Control Patches
© Kodak, 2007 TM: Kodak
Blue
Cyan
Green
Yellow
Red
Magenta
White
3/Color
Black
Kodak Gray Scale
C
Y
M
© Kodak, 2007 TM: Kodak
A 1 2 3 4 5 6 M 8 9 10 11 12 13 14 15 B 17 18 19